ISBN 978-82-326-3646-4 (printed version)
ISBN 978-82-326-3647-1 (electronic version)
ISSN 1503-8181

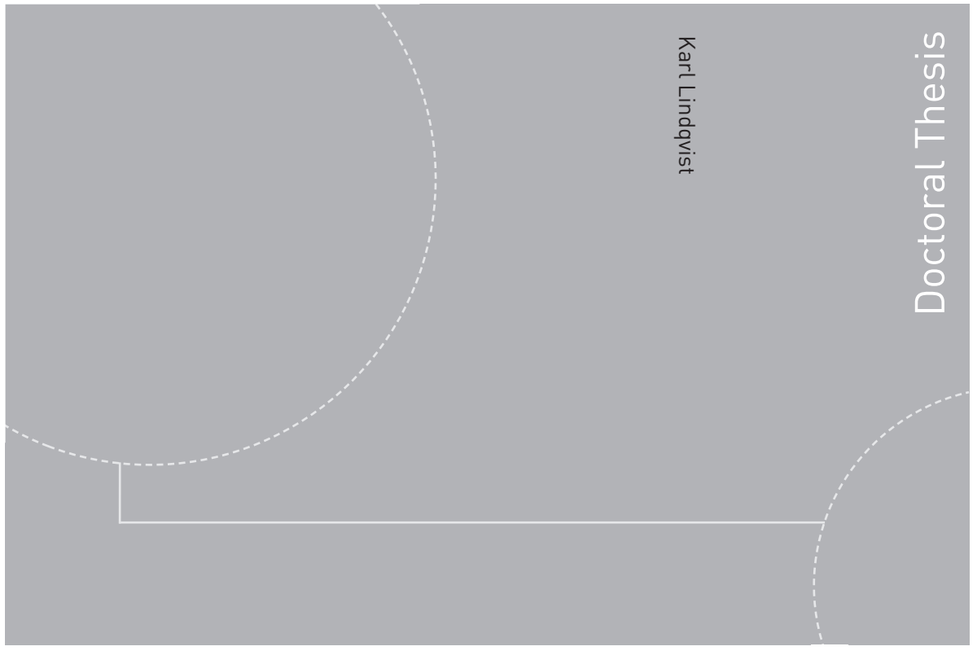

Doctoral theses at NTNU, 2019:18

Karl Lindqvist

Computational Fluid Dynamics Modeling of Flow and Heat Transfer in Fin-Tube Bundles

NTNU
Norwegian University of
Science and Technology
Faculty of Engineering
Department of Energy and Process Engineering

NTNU
Norwegian University of
Science and Technology

Doctoral theses at NTNU, 2019:18

NTNU

NTNU
Norwegian University of
Science and Technology

Karl Lindqvist

Computational Fluid Dynamics Modeling of Flow and Heat Transfer in Fin-Tube Bundles

Thesis for the degree of Philosophiae Doctor

Trondheim, January 2019

Norwegian University of Science and Technology
Faculty of Engineering
Department of Energy and Process Engineering

NTNU
Norwegian University of
Science and Technology

NTNU
Norwegian University of Science and Technology

Thesis for the degree of Philosophiae Doctor

Faculty of Engineering
Department of Energy and Process Engineering

ISBN 978-82-326-3646-4 (printed version)
ISBN 978-82-326-3647-1 (electronic version)
ISSN 1503-8181

Doctoral theses at NTNU, 2019:18

Printed by Skipnes Kommunikasjon as

Summary

Steam bottoming cycles, powered by gas turbine exhaust heat, are considered for offshore applications as a means of increasing the energy efficiency of power supply and reducing CO_2 emissions from oil and gas production. Strict requirements on volume and weight of the steam generator means that unconventional heat exchanger designs must be considered. This calls for an extension of the validity range of existing thermal-hydraulic correlations for fin-tube bundles (the predominant heat exchanger type in this application) so that designs can be optimized for weight. The aim of the present work is therefore to develop and validate a computational fluid dynamics model of heat transfer and pressure drop in solid- and serrated-fin tube bundles, and use it to expand the region of geometric parameters for which the thermal-hydraulic performance of finned tube bundles is known.

Firstly, a numerical model (grid generation, domain selection, turbulence modeling and solution method) is established and validated against experimental data for four different fin tube geometries, two with plain fins and two with serrated fins. This study is the first in open literature to simultaneously address grid convergence of the variables of engineering interest and comparison with experimental data of the same variables (and not just correlations). Predicted heat transfer and pressure drop data are within, or very close to, the experimental uncertainty for all four cases, with maximum root mean square errors of 13.8 % and 14.4 % respectively. It is therefore considered acceptable to use the numerical method in lieu of experimental measurement to produce data for correlation development.

The numerical model is coupled to an iterative adaptive sampling method, and combined with experimental data from open literature, to produce improved correlation for heat transfer and pressure drop with maximum impact per added data point. The root mean square errors (RMSE) of the developed correlations are reduced from 28% and 33% to 15% and 25% for pressure drop and heat transfer, respectively, compared to regression on experimental data only. The correlations are demonstrated to produce a different geometric configuration compared to a reference correlation set, when applied to a test case for weight minimization.

Fin efficiency prediction has received particular attention in this work due to its importance for design, and the relative ease at which it can be computed from first principles in a numerical simulation. The theoretical fin efficiency model is evaluated, along with proposed corrections to account for uneven distribution of the heat transfer coefficient. Correction equations are shown to be in significant error for a tall plain fin geometry. Further investigations reveals two main parameters that influence the accuracy of the theoretical fin efficiency model in extreme cases: The per-row thermal effectiveness and flow bypassing the aperture between the fins.

Parameter studies show that the direction of heat flow (gas heating or gas cooling) and the fin type (annular or helically wound) can be quite important for thermal-hydraulic performance. Specifically, pressure drop can be 25 % higher for spiral fin-tubes under gas heating conditions than for equivalent annular fin-tubes under gas cooling conditions, which is not considered by most correlations. The upstream turbulence level, on the other hand, is of negligible importance. The effect of the number of streamwise tube rows is significant for shallow tube bundles, but is well modeled by some existing correlations.

Finally, the numerical model is extended to the time domain and used to predict vortex shedding in a compact tube bundle. The work demonstrates that vortex suppression does not occur even if fins are added to the tubes, and that the vortex shedding frequency and amplitude is well described by equations developed for bare tube bundles, when an effective diameter is used to account for the fins.

Preface

This thesis is submitted in partial fulfillment of the requirements for the degree of philosophiae doctor (PhD) at the Norwegian University of Science and Technology (NTNU).

The work presented in this thesis has been performed at the Department of Energy and Process Engineering, within the COMPACTS project hosted by SINTEF Energy Research. Special thanks are due to my supervisors, Professor Erling Næss and Dr. Geir Skaugen, for fruitful discussions and valuable input in the course of this project.

During my PhD studies I had the privilege of visiting Professor Nikolaos Sahinidis' group at Carnegie Mellon University. I am grateful for this opportunity, and the hospitality shown to me during my stay.

I would like to thank my colleagues at EPT for a great work environment, social activities and lunch discussions. Special thanks to the ComKin & Friends group for good times, and to Tian and Christoph in particular for our CFD and OpenFOAM discussions. I must also mention my A514 colleagues and my office mates at CMU. It's been a privilege to get to know you!

Finally, I am indebted to my wife Louise for all the support, patience and encouragement during these years. It's an honor sharing life with you.

Contents

Nomenclature

Note that additional nomenclature is given in chapters 4–7.

Roman letters

A	heat transfer area [m^2]
d_o	bare tube outer diameter [m^2]
h_f	fin height [m]
m	nondimensional fin parameter ($=\sqrt{2\alpha/(\lambda t_f)}$) [-]
N_r	number of tube rows [-]
$\dot{Q}$	heat flow [W]
T	temperature [K]
$u_{F_{min}}$	mean velocity in minimum free flow area [$\mathrm{m\,s^{-1}}$]

Greek letters

α	heat transfer coefficient [$\mathrm{W\,m^{-2}\,K^{-1}}$]
ϵ	thermal effectiveness ($=q/q_{\max}$) [-]
η_f	fin efficiency [-]
λ	thermal conductivity [$\mathrm{W\,m^{-1}\,K^{-1}}$]
ν	kinematic viscosity [$\mathrm{m^2\,s^{-1}}$]
ρ	density [$\mathrm{kg\,m^{-3}}$]

Subscripts

b	bulk, mixing cup
f	fin
t	tube
w	wall

Dimensionless numbers

$\mathrm{Re} = \frac{u_{F_{\min}} d_o}{\nu}$	Reynolds number
$\mathrm{Eu} = \frac{\Delta p}{N_r \frac{1}{2} \rho u^2_{F_{\min}}}$	Euler number
$\mathrm{Nu} = \frac{\alpha d_o}{\lambda}$	Nusselt number

Chapter 1

Introduction

Increased energy efficiency in the industrial sector is identified as one of the key measures that can deliver a peak in global energy-related greenhouse gas emissions without changing economic prospects [1]. This has also been highlighted in *Norway´s Technology Strategy for the 21st Century*, where one out of four strategic goals are to: "Maintain the Norwegian position as the oil and gas province with the highest energy efficiency, the lowest level of emissions to air, and lowest harmful discharges to sea per produced unit."[2].

Offshore oil- and gas production is energy intensive due to the large amount of power required for reservoir pressure support (water/gas injection), export gas compression (for natural gas fields) and other utilities. The power is usually supplied by several gas turbine engines (30-40 MW each) in simple cycle configuration; Heat recovery from the exhaust of these engines is, in many cases, a low hanging fruit in terms of increased energy efficiency. Implementing bottoming cycles to produce power from exhaust heat would be impactful, since power production is the single largest source of CO_2 emissions from individual platforms. The overall CO_2 emissions reduction potential per installation is about 25 % [3]. The waste heat recovery units (WHRUs) which are part of these bottoming cycles must, however, meet stringent requirements on size, weight and durability in order to be attractive for offshore use. Widespread installation has not taken place - only three production facilities are currently using bottoming cycles for power production on the Norwegian continental shelf [4].

Earlier work on the design of offshore bottoming cycles has indicated that small diameter fin-tubes lead to lower weight and volume of the WHRU [5]. Meanwhile, experimental work and correlation development has primarily focused on the large diameter tubes that are relevant for onshore heat recovery. Compact geometries have been tested for air cooler applications, but geometric details and materials selection are different (crimped fins are common) as well as the

operating conditions (dehumidifying or frosting conditions are often considered). This leads to a need for extended validity ranges of thermal-hydraulic correlations that can be used in design optimizations, which in turn calls for more data on compact fin-tube geometries.

Using Computational Fluid Dynamics modeling, rather than experimental testing, to produce these data has several advantages. Firstly, all comparisons are made on a consistent basis, e.g. with regards to geometric representation, thermophysical properties and data reduction. By contrast, this is not true in general for comparisons of experimental studies performed by different research groups. Secondly, it is possible to model geometries that are difficult to physically manufacture and therefore to cover the entire interesting parameter space. Thirdly, simulations can be time efficient, not only in terms of lead time from start to finish but also due to the fact that many simulations can be run in parallel on compute clusters. The time efficacy is, however, contingent on having a rational and possibly automated simulation setup.

As regards reliability, there has been speculation as to whether flow-induced vibrations can occur in fin-tube bundles. This is, of course, an even more important question when small diameter tubes are considered, due to the lowered bending stiffness. A large body of knowledge has been produced on flow induced vibrations in bare tube arrays, due to its importance in nuclear power production. It is beyond the scope of this work to check if all design rules for bare tube bundles are transferable to fin-tube bundles. The thermal-hydraulic CFD model can, however, easily be extended to study some phenomena and thus give an indication as to if more research is needed.

1.1 Research objectives and scope

The main scientific objective of the present work is to develop and validate a computational fluid dynamics model of solid- and serrated-fin tube bundles and use it to expand the region of geometric parameters for which the engineering performance of finned tube bundles is known. The study is limited to a staggered equilateral triangular tube layout (the most compact arrangement). The sub-objectives supporting this task are:

- To validate the model against in-house thermal-hydraulic experimental data
- To vary key geometric parameters systematically, identify thermal-hydraulic trends, and use the tool predictively to extrapolate into regions of particular interest (e.g. small diameter serrated fin-tubes).
- To critically evaluate correlations from the literature and construct new correlations from numerical data as well as existing experimental data
- To extend the model to study flow induced vibrations

1.2 Contribution

The progression between the articles that constitute this thesis, and the main conclusions from them, can be summarized as follows:

1. Karl Lindqvist and Erling Næss. "A validated CFD model of plain and serrated fin-tube bundles". In: *Applied Thermal Engineering* 143 (2018), pp. 72–79. ISSN: 13594311. DOI: 10.1016/j.applthermaleng.2018.07.060

   This paper establishes the numerical model and presents validation and grid convergence of the methodology. It is indicated that established correlations have poor predictive accuracy for small diameter tubes, though this could not be concluded at this stage. Calculations also demonstrate that the Weierman and Hashizume fin efficiency corrections are not sufficient to correct the fin efficiency for non-ideal conditions.

2. Karl Lindqvist and Erling Næss. "On correction factors in thermal-hydraulic correlations for compact fin-tube bundles (submitted)". In: *Heat and Mass Transfer* (2018)

   The numerical model is used to study the sensitivity to five parameters which have not yet been studied experimentally or numerically. Three of them are concluded to be important for compact fin-tube bundle modeling, namely the fin efficiency prediction, the fin pitch and the modeling of variable thermophysical properties. We hypothesize that flow bypassing the gap between the fins (flowing outside the fin diameter) plays an important role in fin efficiency deviating from the theoretical fin efficiency. The analysis was enabled by computing the exact fin efficiency numerically, without restrictive assumptions on e.g. the bulk temperature.

3. Karl Lindqvist et al. "A machine learning approach to correlation development applied to fin-tube bundle heat exchangers". In: *Energies* 11.12 (2018). DOI: 10.3390/en11123450

   The numerical model is coupled to ALAMO, a correlation development software that implements statistical- and machine learning algorithms. Existing experimental data and new numerical simulation data is combined to create improved correlations for heat transfer and pressure drop. Adaptive sampling is used to maximize the benefit of each numerical simulation. The impact of the new correlations is demonstrated on a boiler test case. CFD simulations are also used to validate the correlations and to discuss trends in the design variables. A main conclusion, apart from the correlations themselves, is that the Nusselt number depend primarily on the Reynolds number and the tube diameter. Reference correlations are conclusively shown to have poor predictive accuracy in the region of compact fin-tube bundles.

4. Karl Lindqvist and Erling Næss. "Numerical Modeling of Vortex Shedding in Helically Wound Finned Tube Bundles in Cross Flow". In: *Proceedings of the 16th International Heat Transfer Conference (IHTC-16)*. Beijing, China, 2018

   The numerical model is extended to the time domain and used to predict vortex shedding in a compact tube bundle. The work demonstrates that vortex suppression does not occur even if fins are added to the tubes, and that the vortex shedding frequency and amplitude is well described by equations developed for bare tube bundles, where an effective diameter is used to account for the fins. Heat transfer is not considered in these simulations.

References

[1] International Energy Agency. *WEO 2015 Special Report on Energy and Climate Change - Executive Summary*. Tech. rep. Paris: IEA Publications, 2015, p. 10.

[2] OG21 - Oil and Gas in the 21st Century. *Norway´s Technology Strategy for the 21st Century*. Tech. rep. Oslo, 2013.

[3] Marit Jagtøyen Mazzetti et al. "Energy-Efficiency Technologies for Reduction of Offshore CO2 Emissions". In: *Oil and Gas Facilities* 3.01 (2014), pp. 89–96. ISSN: 2224-4514. DOI: 10.2118/169811-PA.

[4] P Kloster. "Energy Optimization on Offshore Installations with Emphasis on Offshore Combined Cycle Plants". In: *Offshore Europe Oil and Gas Exhibition and Conference*. Society of Petroleum Engineers, 1999. DOI: 10.2118/56964-MS.

[5] G. Skaugen et al. "Design and optimization of waste heat recovery unit using carbon dioxide as cooling fluid". In: *Proceedings of the ASME 2014 Power Conference*. 2014, pp. 1–10.

[6] Karl Lindqvist and Erling Næss. "A validated CFD model of plain and serrated fin-tube bundles". In: *Applied Thermal Engineering* 143 (2018), pp. 72–79. ISSN: 13594311. DOI: 10.1016/j.applthermaleng.2018.07.060.

[7] Karl Lindqvist and Erling Næss. "On correction factors in thermal-hydraulic correlations for compact fin-tube bundles (submitted)". In: *Heat and Mass Transfer* (2018).

[8] Karl Lindqvist et al. "A machine learning approach to correlation development applied to fin-tube bundle heat exchangers". In: *Energies* 11.12 (2018). DOI: 10.3390/en11123450.

[9] Karl Lindqvist and Erling Næss. "Numerical Modeling of Vortex Shedding in Helically Wound Finned Tube Bundles in Cross Flow". In: *Proceedings of the 16th International Heat Transfer Conference (IHTC-16)*. Beijing, China, 2018.

Chapter 2

Background

Fin-tube bundle thermal engineering is, arguably, a well developed and disseminated field both in textbooks and in the research literature. How can further research be warranted, if at all needed? At least three arguments can be made based on observation:

- Theoretical (mathematical) modeling of fin-tubes is developed to conform to equivalent models for other heat transfer surfaces, rather than to maximize accuracy.
- Publicly available experimental data is inconsistent due to varied experimental setups and data reduction practices. Uncertainty analyses are often lacking or incomplete, which complicates use of the data.
- Theoretical and empirical work on flow induced vibrations have largely considered bare tube arrays. The extent to which models are applicable to finned tubes is uncertain.
- Computational Fluid Dynamics models have not been used to their full potential to address the previous shortcomings.

This chapter is intended to provide some evidence to these statements and show how they relate to this thesis work.

2.1 The theoretical framework for convective heat transfer

The engineering treatment of convective heat transfer from a surface with area A to a fluid of bulk temperature T_b is straightforward: The heat flux is proportional to the temperature difference between the surface and the fluid with the heat

transfer coefficient α introduced as the proportionality constant, viz.

$$\frac{\dot{Q}}{A} = \alpha(T_w - T_b) \tag{2.1}$$

A few complications arise for fin-tube bundle heat exchangers:

1. The heat transfer area consists of a bare tube area A_t and a fin area A_f, the latter of which has an additional heat transfer resistance due to heat conduction through the fin. As a consequence, the fin temperature is not equal to T_w, and a fin efficiency η_f must be introduced.
2. The heat transfer coefficient is not uniform across A, particularly not in the wake behind the tube. This leads to inaccuracies in fin efficiency calculations, since the theoretical fin efficiency model assume a uniform α. Corrections and/or solutions for uneven distribution is not trivial, and very little empirical data (local heat flux measurements etc.) is available. The uniformity assumption also adds some bias in correlations for α itself, since it is the case that not all of A will experience an increased α from, say, an increased flow velocity. The tube wake is again the most prominent example.
3. The flow though a tube bundle is not homogeneous across its cross-section; Part of the flow may pass outside the fin diameter (particularly if fins are packed very densely), which means that the bulk temperature in Equation 2.1 becomes an inaccurate measure of the driving force for heat transfer

This thesis does not challenge Equation 2.1 or propose an alternative formulation. Doing so might be worthwhile, but would require re-evaluation of all experimental literature published to date. Instead, this thesis explores the domain of validity of Equation 2.1 and improves upon the prediction of α, given the accuracy constraints of the model. As a teaser, consider the error in average observed (calculated) fin efficiency, compared to the analytical fin efficiency, of a rectangular fin array with bypassing flow, Figure 2.1. This calculation assumes a constant heat transfer coefficient and integrates the transferred heat along the flow length of the fin (500 intervals), using an analytical fin efficiency solution [1] locally. The observed fin efficiency is evaluated as

$$\eta_f = \frac{\sum \dot{Q}/\Delta T_{LM}}{\sum \dot{Q}^*/\Delta T^*_{LM}} \tag{2.2}$$

where the asterisk denotes a solution with infinite thermal conductivity of the fin. This procedure eliminates inaccuracies related to complications number 1 and 2 above. Yet, the observed fin efficiency differs fundamentally from the theoretical one even under otherwise ideal conditions.

The magnitude of the error is dependent on the thermal effectiveness ϵ (i.e. the length of the fin in the flow direction) which in this case has a high value

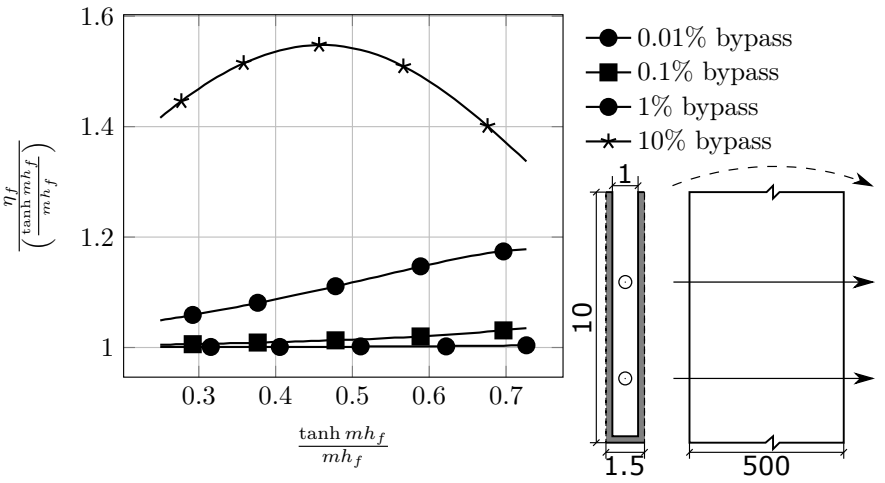

Figure 2.1: Error in theoretical fin efficiency of 0.5 mm thick parallel carbon steel fins, where part of the mass flow through the 1×500 mm channels does not take part in heat transfer (is bypassed). Reynolds number range (hydraulic diameter): 2 000 - 50 000; constant Nusselt number (fully developed turbulent flow)

(about 90 %). The issue is therefore relevant for compact fin-tube bundles where the per-row thermal effectiveness can be quite high in an effort to reduce the number of tube rows.

2.2 Experimental studies and their accuracy

A pertinent question for this thesis work has been how existing experimental data can be leveraged to reach the objectives outlined in the introduction. One particular challenge is that the experimental uncertainty often is unknown or incompletely reported in journal publications. Several studies, such as [2], claim an uncertainty of about 5 % for the Nusselt number without further demonstration. Holfeld [3], meanwhile, calculated that the heat transfer coefficient is shifted ±3–6 % higher when taking into account the welding bond failure provisions that are allowed according to current welding standards, compared to assuming that all fins are perfectly attached. While measurement techniques may vary, it is hard to imagine that studies that claim less than 5 % error in Nusselt number have accounted for all relevant uncertainties. A similar reasoning applies to Euler number uncertainties, which tend to increase exponentially at lower Reynolds numbers due to uncertainties in both the measured flow velocity and the pressure drop

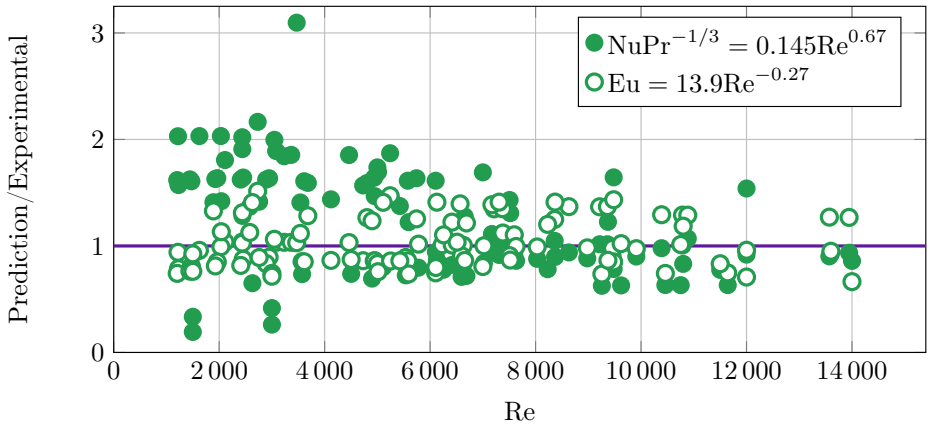

Figure 2.2: Predictive accuracy of Nusselt and Euler numbers as a simple power function of Re (indicated in legend), with constants calibrated to experimental data, compared to the underlying data itself. Data from various authors in open literature, extracted from in-house database.

itself. Reporting an artificially low uncertainty (e.g. the uncertainty at the largest Reynolds number) is unhelpful and misleading. This has implications for model validation, since it is useful and appropriate to compare not only model output with experiment output, but also model output with experimental uncertainty range (and, preferably, the model uncertainty range as well). The solution in this thesis work has been to use in-house data for parts of the validation (where uncertainties have been thoroughly analyzed) and to assume a reasonable average uncertainty of 10 % for Nusselt number and 15 % for the Euler number for external (published) data.

A second challenge in using experimental data is the considerable scatter that can be observed after correcting for the Reynolds number dependency (Figure 2.2). The data spread may be due to some underlying function of the fin-tube bundle geometry, but it could also (at least partially) be attributed to inconsistent experimental setups and data reduction methods. Considering the previously mentioned challenge with obtaining good uncertainty measures, it would be hard to discriminate between good- and poor quality data. At the same time, the experimental data is needed to develop improved correlations, since it would be tremendously time-consuming to reproduce all the required data using CFD simulations. The simplistic approach taken in this work has been to analyze the data statistically in the software ALAMO [4] and run CFD simulations in regions of

expected high uncertainty. Further details on this work is given in the correlation development paper (Paper 3).

2.3 Numerical studies

Numerical studies of fin-tube bundles started to emerge in the late 1990's and early 2000's as computational power grew and as CFD transitioned from a research topic in itself to an engineering tool capable of handling complex geometries. As shown in Table 2.1, increases in geometrical representation, model sizes and simulation refinement has largely followed the rapid increase in computational power (i.e. Moores law) available to the heat transfer researchers. Early studies modeled few tube rows, used 1^{st} order upwind schemes and did not resolve the boundary layers. Publications from one particular author state that qualitative flow features were the primary aim of the investigations [5, 6], and admits that the turbulent Prandtl number was modified by almost 300 % to match simulations with experimental data [7]. Later studies, however, have shown that CFD predictions can be about as accurate as that of correlations, without such a modification [8].

A notable advancement from the early studies was the modeling of serrated, helically wound fins. These geometries are substantially harder to model compared to plain annular fins due to the large number of small features on serrated fins, and the inherent asymmetry of the helix. It is plausible to assume that this increased model complexity caused the reduced number of modeled tube rows that occurs simultaneously. It is only relatively recently that Ó Cléirigh and Smith [8] simulated a full 8 row tube bundle with serrated, helically finned tubes.

No clear trend is observed regarding turbulence model selection, other than the prevalence of the RNG and Realizable k-ε models. A thorough and consistent comparison of various turbulence models is lacking in the literature; Nemati and Moghimi [9], though aspiring to present such a comparison, did not use a consistent computational grid for all models and did not report the numerical setup. It is therefore likely that turbulence models have been selected based on factors other than accuracy, such as ease of convergence.

The terms Grid Convergence and Quantitative Experimental Validation in Table 2.1 require careful definition in the context of predictive CFD. At the least, grid convergence requires statements or demonstration of

- the variable monitored for convergence (e.g. the Nusselt number),
- the degree of convergence achieved (e.g. <5 %) and
- the tested change(s) in grid resolution for which convergence was observed.

Table 2.1: Numerical studies of staggered fin-tube bundles published in open literature (top) and this thesis' contributions (bottom)

Ref.	NSSG[1]	Re range [$\cdot 10^3$]		N_r	Fin type				Turbulence model	Wall model	Scheme order	GC[2]	QEV[3]
		min	max		solid	serrated	annular	helical					
[10]	2	2	8	4	✓		✓		Laminar	-	1st		✓
[11]	14	5	70	4	✓		✓		RNG k-ε	wall fcn	1st		
[12]	5	8.6	43	4	✓		✓		RNG k-ε	?	1st		
[7]	1	5	18	6	✓		✓		Realizable k-ε	resolved	2nd		
[13]	3	20	1000	1		✓		✓	k-ε	?	2nd		
[14]	5	3.5	50	1	✓	✓	✓	✓	RNG k-ε	resolved	$\geq$2nd		✓
[5]	2	6	28	1	✓	✓	✓		Realizable k-ε	resolved	2nd		
[6]	1	7	41	2-4		✓	✓		Realizable k-ε	resolved	2nd		
[15]	2	1	5	3	✓	✓		✓	Laminar	-	2nd	✓	
[16]	5	3.5	50	1	✓	✓	✓	✓	RNG k-ε	resolved	$\geq$2nd		✓
[8]	3	5	30	8	✓	✓		✓	k-ω SST	resolved	?	✓	
[9]	1	3.3		4	✓		✓		Various	?	?		
[17]	1	10	24	∞		✓		✓	RNG k-ε	?	1st		
[18]	1	10		6		✓		✓	RNG k-ε	?	3rd		
[19]	1	10		6/∞		✓		✓	RNG k-ε	?	3rd		
[20]	4	5	50	∞	✓	✓		✓	S-A	resolved	2nd	✓	✓
[21]	70+30	0.5	19	∞	✓	✓		✓	S-A	resolved	2nd		
[22]	1;4;40	0.5	50	8/∞	✓	✓	✓	✓	S-A	resolved	2nd		
[23]	2	5		∞	✓			✓	S-A	resolved	2nd	✓	

1) Number of Simulated Staggered Geometries
2) Grid Convergence
3) Quantitative Experimental Validation

Monitoring an irrelevant variable, or performing a negligibly small (or undocumented) change in grid resolution, are two omissions of grid convergence checks that still occur occasionally in articles covering numerical studies. In practice, second order schemes are required to achieve grid convergence for all variables of engineering interest [24]. Studies that claim (but do not demonstrate) grid convergence with 1st order upwind or hybrid schemes do not pass the "Grid Convergence" check in Table 2.1.

In the same vein, a Quantitative Experimental Validation of the numerical model requires

- comparison of a relevant variable with
- high quality experimental data, preferably with a known uncertainty, and
- no manual adjustments of numerical grid or turbulence modeling constants.

Comparison with correlations are not entirely inappropriate, but introduces the risk of cherry-picking correlations that match the numerical results. Moreover, CFD methods should aspire to achieve a higher accuracy than correlations, which requires better validation data.

It is clear from Table 2.1 that no previous study has adequately demonstrated both grid convergence and quantitative comparison with experimental data simultaneously. The only plausible explanation to this (lack of) focus is that the perceived benefits of CFD has not yet been sufficiently large for it to compete with experimental work. At the very least, there has never been a lack of experimental data against which model validation could have been performed. With increased computational power, however, this balance may change and has already, to some degree, changed.

Finally, note that the first three publications from this work listed in Table 2.1 (i.e. [20, 21, 22]) use the same numerical method. Hence, the grid convergence and validation presented in [20] apply to all three publications.

2.4 Flow induced vibrations

Nuclear power safety and reliability has been a main driver for the research in flow induced vibrations, spurred by a number of unexpected and costly reactor shutdowns. Flow-induced vibrations were found to cause fatigue failures in fuel rods and boiler pre-heater sections, establishing a need for fundamental phenomenological understanding and reliable design criteria [25]. Vast experimental efforts have since been put into characterizing single phase liquid flow over bare tube arrays, as well as extensions to various geometrical configurations and flow types. This has led to a set of design criteria and stability maps for bare tube heat exchangers [26]. The vibration excitation mechanisms for tube bundles in cross-flow configuration are generally divided as follows [27]:

- Fluid-elastic instability
- Periodic wake (vortex) shedding
- Turbulence excitation
- Acoustic resonance

Fluid-elastic instability and acoustic resonance are the most important vibration mechanisms for gaseous flow, according to Pettigrew et al. [28]. Vortex shedding is judged as unlikely, but turbulence excitation is possible.

Studies on flow induced vibrations in fin-tube (rather than bare tube) bundles are relatively scarce. Lumsden and Weaver [29] and Wang and Weaver [30] measured the fluid-elastic stability limit of four different fully flexible arrays of serrated finned tubes. The addition of dense fins to otherwise identical bare tubes were found to stabilize the parallel triangular tube- and inline square tube layouts. The rotated square tube- and normal triangular tube layouts, on the other hand, were de-stabilized by the addition of fins. In all cases,however, the stability maps for bare tube arrays were found to be conservative with respect to the onset of fluid-elastic instability for the finned tubes. Previous work on vortex shedding from high-finned tubes has concentrated on single and tandem tubes rather than tube arrays [31, 32, 33]. In these cases, the fins can be accounted for by introducing an effective diameter. The corresponding phenomenon has not been studied in fin-tube *bundles*, to the authors' knowledge.

The importance of flow-induced vibrations can be expected to increase as weight optimized WHRUs are considered. Weight reduction may lower the structural rigidity of the tube bundle by employing smaller diameter tubes, fewer support plates and higher gas velocities. It is therefore essential that current models for flow induced vibrations are critically evaluated such that vibration problems (and resulting damage, e.g. from fretting or fatigue) are avoided at the design stage.

2.5 Knowledge gaps

In light of the state-of-the-art it can be concluded that

- Present thermal-hydraulic design correlations have evolved from decades of experimental work, not all of equal quality or consistency. Data scatter prevents a thorough examination of trends with respect to changes in geometry.
- Fin efficiency prediction can be difficult due to the unrealistic (but necessary) assumption of a uniform heat transfer coefficient.
- Closely packed small diameter fin-tubes are promising for offshore use, but these geometries are outside the validity range of current correlations. There

are insufficient experimental data to construct new design correlations without further work.

- Numerical methods are able to predict thermal-hydraulic performance to some degree, but most studies lack thorough validation with experiments.
- Fluid-elastic instability of finned tube bundles have been studied experimentally, but only for very specific geometries. Vortex shedding has also been studied, but only for single- and tandem fin-tubes. The design rules developed for bare tube arrays have not been extensively applied to finned tube arrays in open literature.

Enabling the design and optimization of compact and lightweight heat recovery units is primarily a matter of generating new data. New data, in turn, enables evaluation of present design rules and correlations and development of new ones.

This work addresses these knowledge gaps by, firstly, establishing a numerical model that can be used for quantitative studies of heat transfer of pressure drop in lieu of experimental measurements. It is the first to demonstrate both a grid convergence analysis and quantitative comparison with experimental data for fin-tube bundles. Thus, the efficacy of each of the key components of the model is also confirmed:

- Steady RANS modeling of the flow field, with a one-equation turbulence model (Spalart-Allmaras)
- Parameterized hexahedra-dominated hybrid grid for plain- and serrated fin-tubes
- Choice of computational domain, specifically the reduced domain model where a small section of an "infinite" tube bundle is modeled

For details, refer to chapter 3 and Paper 1.

Secondly, the model is used to produce data with the specific aim of improving correlations for compact fin-tube bundles. The problem lends itself well to statistical treatment due to the relatively large number of geometric parameters to be modeled (at least 5, excluding the flow velocity) as well as the scatter in existing experimental data. Given the advantages of CFD modeling (consistency, relative time efficacy and geometric freedom), it is interesting to consider an automated, iterative correlation development approach that makes use of machine learning concepts. In particular, it is possible to estimate regions in the parameter space where correlation outputs (heat transfer and pressure drop coefficients) are uncertain, and suggest a CFD simulation in such a region. This approach maximizes (at least in principle) the impact that each added data point has on the final correlation accuracy. Results from this approach is presented in Paper 3, along with a thorough sensitivity analysis of the correlation outputs with respect to the various geometric input parameters.

Thirdly, the model is used to study specific aspects of fin-tube thermal-hydraulic modeling that has received comparatively little attention in the literature. Paper 2 presents findings related to the direction of heat flow (gas heating or gas cooling), the fin type (annular or spirally wound), the fin efficiency, the fin pitch, the number of streamwise tube rows and the inlet turbulence level. A particular strength of the numerical approach is the ability to perform simulations with infinite thermal conductivity of the fin, and hence deduce the fin efficiency without additional assumptions (other than those inherent in the RANS model). The format of this study is primarily a traditional parameter study. The fin efficiency, however, is investigated using a Latin Hypercube sample such that the entire design space is covered. Further analysis is then performed for two geometries of particular interest.

Lastly, the model is extended into the time domain, to enable analysis of vibration-related research questions.

References

[1] A D Kraus. *Extended surfaces*. Baltimore, MD: Spartan Books, 1964.

[2] Youfu Ma et al. "Experimental investigation of heat transfer and pressure drop in serrated finned tube banks with staggered layouts". In: *Applied Thermal Engineering* 37 (2012), pp. 314–323. ISSN: 13594311. DOI: 10.1016/j.applthermaleng.2011.11.037.

[3] Anna Holfeld. "Experimental investigation of heat transfer and pressure drop in compact waste heat recovery units". PhD thesis. Norwegian University of Science and Technology, 2016.

[4] Alison Cozad, Nikolaos V. Sahinidis, and David C. Miller. "Learning surrogate models for simulation-based optimization". In: *AIChE Journal* 60.6 (2014), pp. 2211–2227. ISSN: 15475905. DOI: 10.1002/aic.14418.

[5] Stuart Russel McIlwain. "A Comparison of Heat Transfer Around a Single Serrated Finned Tube and a Plain Finned Tube". In: *International Journal of Research & Reviews in Applied Sciences* 2.February (2010), pp. 88–94.

[6] Stuart Russel McIlwain. "A CFD Comparison of Heat Transfer and Pressure Drop Across Inline Arrangement Serrated Finned Tube Heat Exchangers With an Increasing Number of Rows". In: *International Journal of Research & Reviews in Applied Sciences* 4.August (2010), pp. 162–169.

[7] Stuart Russel McIlwain. "Improved Prediction Methods for Finned Tube Bundle Heat Exchangers in Crossflow". PhD thesis. University of Strathclyde, 2003.

[8] Cathal T. Ó Cléirigh and William J. Smith. "Can CFD accurately predict the heat-transfer and pressure-drop performance of finned-tube bundles?" In: *Applied Thermal Engineering* 73.1 (2014), pp. 681–690. ISSN: 13594311. DOI: 10.1016/j.applthermaleng.2014.08.019.

[9] Hossain Nemati and Mohammad Moghimi. "Numerical Study of Flow Over Annular-Finned Tube Heat Exchangers by Different Turbulent Models". In: *CFD Letters* 6.3 (2014).

[10] Jiin-Yuh Jang, Jen-Tien Lai, and Long-Chi Liu. "The thermal-hydraulic characteristics of staggered circular finned-tube heat exchangers under dry and dehumidifying conditions". In: *International Journal of Heat and Mass Transfer* 41.21 (1998), pp. 3321–3337. ISSN: 00179310. DOI: 10.1016/S0017-9310(98)00037-4.

[11] Mi Sandar Mon. "Numerical investigation of air-side heat transfer and pressure drop in circular finned-tube heat exchangers". PhD thesis. Technischen Universität Bergakademie Freiberg, 2003.

[12] Mi Sandar Mon and Ulrich Gross. "Numerical study of fin-spacing effects in annular-finned tube heat exchangers". In: *International Journal of Heat and Mass Transfer* 47.8-9 (2004), pp. 1953–1964. ISSN: 00179310. DOI: 10.1016/j.ijheatmasstransfer.2003.09.034.

[13] Marco Torresi et al. "CFD Analysis of the Flow Through Tube Banks of HRSG". In: *Proceedings of ASME Turbo Expo 2008, Berlin, Germany*. 2008, pp. 1–11.

[14] Rene Hofmann. "Experimental and Numerical Air-Side Performance Evaluation of Finned-Tube Heat Exchangers". PhD thesis. Technischen Universität Wien, 2009.

[15] A. Lemouedda et al. "Numerical investigations for the optimization of serrated finned-tube heat exchangers". In: *Applied Thermal Engineering* 31.8-9 (2011), pp. 1393–1401. ISSN: 13594311. DOI: 10.1016/j.applthermaleng.2010.12.035.

[16] Rene Hofmann and Heimo Walter. "Experimental and Numerical Investigation of the Gas Side Heat Transfer and Pressure Drop of Finned Tubes—Part II: Numerical Analysis". In: *Journal of Thermal Science and Engineering Applications* 4.4 (2012), p. 041008. ISSN: 19485085. DOI: 10.1115/1.4007125.

[17] E. Martinez et al. "Numerical simulation of turbulent air flow on a single isolated finned tube module with periodic boundary conditions". In: *International Journal of Thermal Sciences* 92 (2015), pp. 58–71. ISSN: 12900729. DOI: 10.1016/j.ijthermalsci.2015.01.024.

[18] E. Martinez-Espinosa, W. Vicente, and M. Salinas-Vazquez. "Numerical Analysis for Saving Fin Material in Helical Segmented-Tubes". In: *Applied Thermal Engineering* 110 (2017), pp. 306–317. ISSN: 13594311. DOI: 10.1016/j.applthermaleng.2016.08.061.

[19] Eliseo Martinez-Espinosa et al. "Numerical Analysis of Turbulent Flow in a Small Helically Segmented Finned Tube Bank". In: *Heat Transfer Engineering* 38.1 (2017), pp. 47–62. ISSN: 0145-7632. DOI: 10.1080/01457632.2016.1156396.

[20] Karl Lindqvist and Erling Næss. "A validated CFD model of plain and serrated fin-tube bundles". In: *Applied Thermal Engineering* 143 (2018), pp. 72–79. ISSN: 13594311. DOI: 10.1016/j.applthermaleng.2018.07.060.

[21] Karl Lindqvist and Erling Næss. "On correction factors in thermal-hydraulic correlations for compact fin-tube bundles (submitted)". In: *Heat and Mass Transfer* (2018).

[22] Karl Lindqvist et al. "A machine learning approach to correlation development applied to fin-tube bundle heat exchangers". In: *Energies* 11.12 (2018). DOI: 10.3390/en11123450.

[23] Karl Lindqvist and Erling Næss. "Numerical Modeling of Vortex Shedding in Helically Wound Finned Tube Bundles in Cross Flow". In: *Proceedings of the 16th International Heat Transfer Conference (IHTC-16)*. Beijing, China, 2018.

[24] Patrick J Roache. *Verification and validation in computational science and engineering*. Albuquerque, New Mexico, USA: Hermosa publishers, 1998. ISBN: 0-913478-08-3.

[25] M.P. Païdoussis. "A review of flow-induced vibrations in reactors and reactor components". In: *Nuclear Engineering and Design* 74.1 (1983), pp. 31–60. ISSN: 00295493. DOI: 10.1016/0029-5493(83)90138-3.

[26] D.S. Weaver and J.a. Fitzpatrick. "A review of cross-flow induced vibrations in heat exchanger tube arrays". In: *Journal of Fluids and Structures* 2.1 (1988), pp. 73–93. ISSN: 08899746. DOI: 10.1016/S0889-9746(88)90137-5.

[27] M. J. Pettigrew and C. E. Taylor. "Vibration analysis of shell-and-tube heat exchangers: An overview - Part 2: Vibration response, fretting-wear, guidelines". In: *Journal of Fluids and Structures* 18.5 (2003), pp. 485–500. ISSN: 08899746. DOI: 10.1016/j.jfluidstructs.2003.08.008.

[28] M. J. Pettigrew et al. "Flow-induced vibration and related technologies in nuclear components". In: *Nuclear Engineering and Design* 131.1 (1991), pp. 81–100. ISSN: 00295493. DOI: 10.1016/0029-5493(91)90319-D.

[29] Robert H. Lumsden and David S. Weaver. "The Effect of Fins on Fluidelastic Instability in In-Line and Rotated Square Tube Arrays". In: *Journal of Pressure Vessel Technology* 132.5 (2010), p. 051302. ISSN: 00949930. DOI: 10.1115/1.4001201.

[30] J. Wang and D. S. Weaver. "Fluidelastic Instability in Normal and Parallel Triangular Arrays of Finned Tubes". In: *Journal of Pressure Vessel Technology* 134.2 (2012), p. 021302. ISSN: 00949930. DOI: 10.1115/1.4004621.

[31] W.A. Mair, P.D.F. Jones, and R.K.W. Palmer. "Vortex shedding from finned tubes". In: *Journal of Sound and Vibration* 39.3 (1975), pp. 293–296. ISSN: 0022460X. DOI: 10.1016/S0022-460X(75)80082-4.

[32] S. Ziada et al. "The effect of fins on vortex shedding from a cylinder in cross-flow". In: *Journal of Fluids and Structures* 21.5-7 SPEC. ISS. (2005), pp. 689–705. ISSN: 08899746. DOI: 10.1016/j.jfluidstructs.2004.12.003.

[33] M. Eid and S. Ziada. "Vortex shedding and acoustic resonance of single and tandem finned cylinders". In: *Journal of Fluids and Structures* 27.7 (2011), pp. 1035–1048. ISSN: 08899746. DOI: 10.1016/j.jfluidstructs.2011.04.011.

Chapter 3

Numerical considerations

The numerical methods used in this work to solve the Reynolds averaged Navier-Stokes equations are well known and covered in several textbooks, e.g. [1]. The source code of the utilized software package, OpenFOAM, is also readily available on the internet. This chapter, therefore, focuses on the two numerical aspects that are unique for this work: Grid generation and turbulence model selection.

3.1 Grid generation

Grid generation is arguably one of the most important parts of applied CFD, since the grid quality impacts both the attainable solution accuracy, the rate of convergence (or lack thereof) and the CPU/memory requirements. Sufficient grid generation has consequently been a substantial focus in the present work.

A few general grid requirements (or rules-of-thumb) have been identified for successful application of CFD with a finite volume discretization:

- Flow physics must be resolved (boundary layers, flow gradients, wakes, geometric details)
- At least 10-15 cells across the velocity- and thermal boundary layers
- Moderate wall-normal cell expansion ratio in boundary layer cells ($\leq 1.2 - 1.3$)
- Smooth transitions in cell size across the domain. Preferably less than 20% size difference between adjacent cells, never more than 50%.
- Low skewness and non-orthogonality (affecting accuracy of gradient reconstruction and face interpolation, respectively)

The following grid generation approaches can be considered for complex geometries such as the ones at hand:

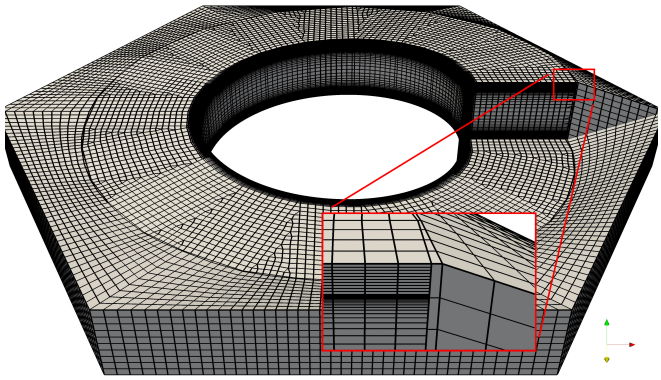

Figure 3.1: Computational grid example, showing hexagonal bulk fluid block and inter-fin grid merged with polyhedral cells (also known as "hanging nodes") at the interface. Periodic interface splitting and merging has not been performed at this stage. Bulk fluid cell size enlarged for clarity.

- Fully structured method
- Cut-cell method
- Unstructured method
- Overset grid method
- Non-conformant grids with interpolation

Several of these methods have been used in the literature. Fully structured grids have been used for annular fin-tube bundles (e.g. [2]), but helical fins have required cut-cell [3], unstructured [4] or non-conformant unstructured [5] grids. Resolving the flow around the individual segments of a serrated fin, while maintaining 10-15 cells through the boundary layer at all Reynolds numbers, is challenging. In addition, periodic flow modeling requires grid matching across the periodic interfaces, which limits the feasibility of some grid generation algorithms. A complicating factor is that small, wedged cells are created when a helical geometry intersects a square domain. Lemouedda et al. [4] solved these challenges by assuming slip walls rather than periodic interfaces transverse to the flow direction. Ó Cléirigh and Smith [5] modeled the fluid between the fins and the fluid outside the fins as two disjoint regions linked by interpolation interfaces. The overset grid method would circumvent some of these problems, but have not yet become as widespread and readily available as the other methods.

The present work has utilized a combination of structured and unstructured block grids to "assemble" a hexahedra-dominated hybrid grid that solves some of

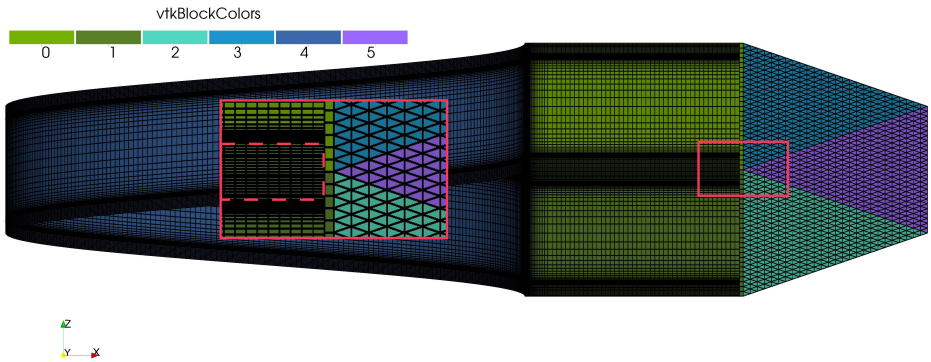

Figure 3.2: Periodic patches (0-3), wall patches (4) and internal faces (5) of the computational grid, showing the cell splitting and merging needed to obtain a continuous, closed computational domain. Dashed line indicates extent of solid (fin) domain.

the mentioned challenges with representing periodic flow around helical, serrated fins (cf. Figure 3.1). An automated, parameterized, grid generation procedure is developed to reduce simulation lead time. The tube array angle is limited to 30° (equilateral triangular layout) to simplify grid generation. This is the most commonly studied array angle in the literature and the most relevant one for compact heat exchangers due to the high packing efficiency.

A hexagonal bulk fluid block around each fin-tube is discretized with hexahedral cells and merged with the boundary layer graded inter-fin grid, creating polyhedral cells (also known as "hanging nodes") at the interface (Figure 3.1). The overlapping patches in the tube wake are then split and merged (Figure 3.2) to create a complete, fully periodic grid with matched cell faces. Finally, the grid around a single fin-tube is merged into a full tube array with inlet- and outlet sections, or a small periodic section of a tube array.

The main features of the computational grid around a typical serrated fin-tube is shown in Figure 3.3. The fluid between the fin segments, where flow separation from the fin surface occurs, is resolved by adding a number of cells through the fin thickness in addition to the existing boundary layer grid (box B). The bulk fluid grid contains a few low quality cells (pyramids and tetrahedra)

in the wake region behind the tube due to the splitting and merging procedure (box C). In return, patch-to-patch interpolation is avoided. The cells are located in an area where flow gradients tend to be small. An unstructured grid is used between the fin segments (box D). A single row of fluid cells is allowed to protrude from the tube surface outwards to avoid pinched cells and cell size jumps at the intersection between adjacent fin segments. This is only relevant for fully serrated fin geometries. Plain fin geometries do not use unstructured cells.

The resulting computational grid satisfy most of the general criteria mentioned earlier in this section. A drawback of the approach includes the reliance on wall functions for the boundary layers on the segment cut sides and on the tip of the individual fin segments. The heat transfer from these surfaces should not be ignored: The fin tip and segment cut side areas of the exemplified geometry in Figure 3.3 are 3.5% and 14.6% of the total heat transfer area per unit length, respectively. However, the tangential velocity as well as the local temperature gradient will be much smaller for the segment cut sides compared to that of the "main" fin surface, which justifies an approximate treatment. These conditions may not pertain at the fin tips; A satisfactory grid convergence was, however, attained even when using wall functions at the fin tips, indicating that the approximate treatment is acceptable at least from a global point of view.

A second drawback is that cell non-orthogonality and skewness of the bulk fluid grid increases as the fin tip clearance approaches zero. This limits the range of this parameter that is possible to simulate to approx. 0.5 mm. The practical impact of this limitation is judged as negligible. Similar limitations would probably occur with other grid generation methods due to cell pinching.

3.2 Solution method

Initial simulations in this project focused on modeling all tube rows in a tube bank, including inlet- and outlet sections, like most earlier published studies have done. In the interest of time efficacy, a further reduction of the modeled fluid domain was considered, inspired by the work of Martinez et al. [6]. The full and reduced domains are shown in Figure 3.4.

The governing equations in a reduced, cyclic domain can be solved by introducing source terms to account for the average pressure drop and heat addition though the domain. The pressure- and temperature fields are, in this case, interpreted as the deviation from the average pressure/temperature gradient imposed by the source term. It was, however, found that iterative stability (i.e. the ability to reach a converged steady state solution) was greatly improved if the streamwise periodic boundary values for pressure and velocity were updated much more seldom than the interior- and transverse boundary values. The periodic problem is, in this way, solved as a series of regular problems with specified inlet veloc-

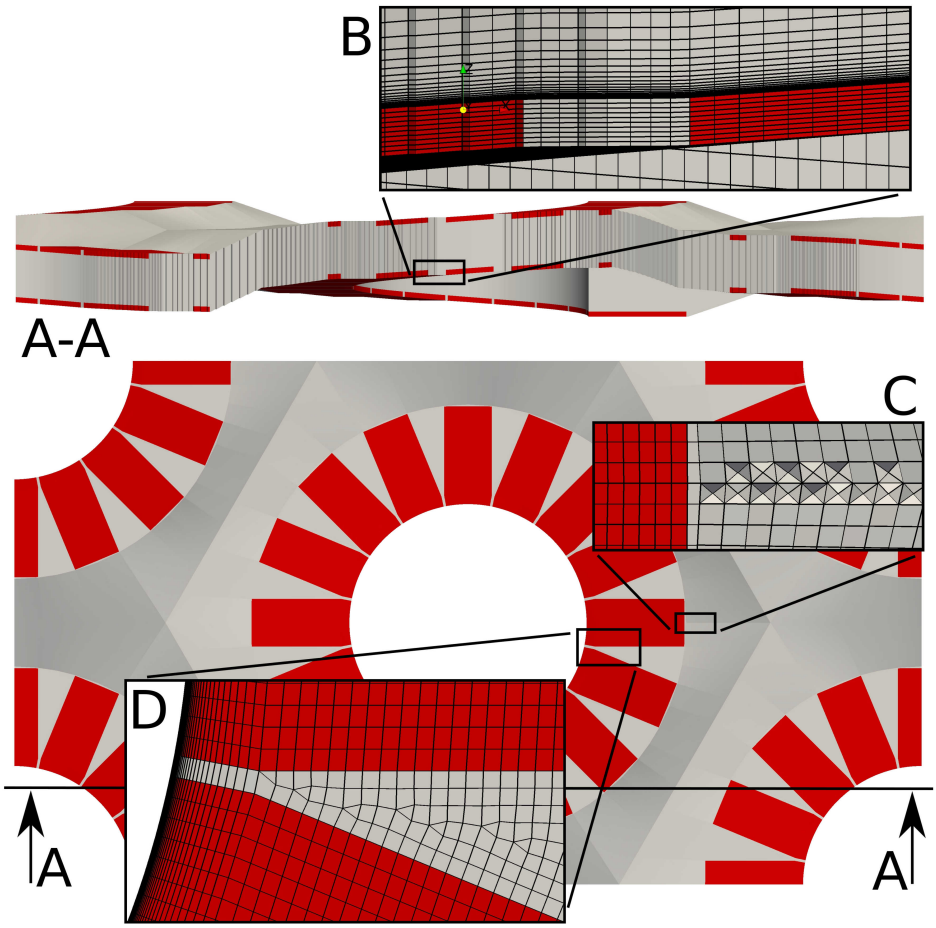

Figure 3.3: Features of the computational grid; Unstructured grid between fin segments and boundary layer grid on fin and tube surfaces (B&D), and cut through patched cells showing pyramid cells (C)

ity and outlet pressure profiles. An additional benefit is that wall conditions for temperature is not limited to a constant heat flux.

Further stability improvements could be demonstrated by avoiding simultaneous update of the outlet pressure and inlet velocity boundary fields. A staggered update was therefore implemented, where updates are spaced with equal period but separated by a constant offset. The profiles for temperature and modified

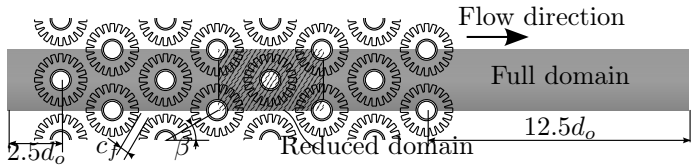

Figure 3.4: Full and reduced computational domain, including array angle, β

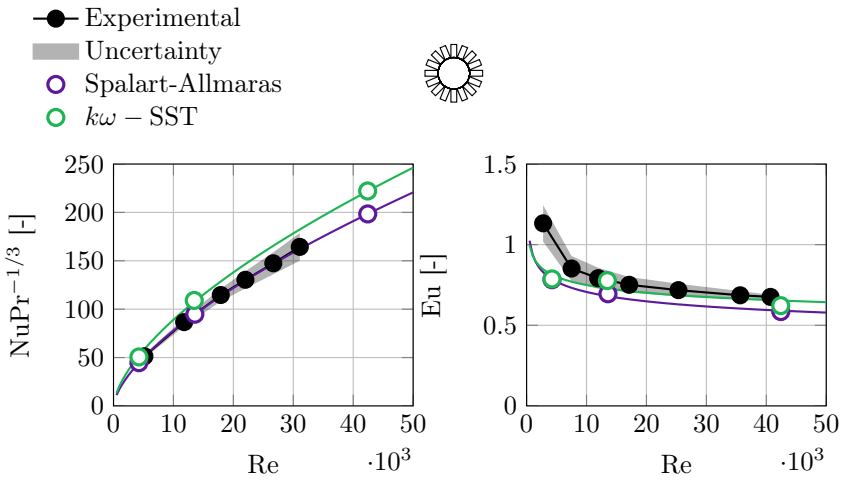

Figure 3.5: Turbulence models

turbulent viscosity are updated every iteration, acting as a fully periodic boundary.

The number of iterations between profile updates are adjusted to ensure convergence. In addition to being copied, profiles for velocity and temperature are scaled to satisfy a specified area average, such that flow rate and temperature difference can be set. Simulations are considered converged when total pressure drop and surface heat fluxes does not change significantly between profile updates, nor with continued iterations. Uniform profiles are used as initial conditions.

3.3 Turbulence modeling

As highlighted in chapter 2, the literature is not quite clear on whether or not the predominant RANS modeling approach is sufficient for thermal-hydraulic predictions of fin-tube bundles. There is, on the other hand, little evidence against it.

Table 3.1: Tube and array geometric parameters used for the turbulence model comparison. Parameter definitions: Figure 3.6)

Reference	[8]
Fin type	serrated
Fin material	steel
d_o [mm]	20.87
h_f [mm]	8.61
h_s [mm]	8.61
t_f [mm]	0.91
s_f [mm]	5.08
w_s [mm]	3.97
β^1 [deg]	30
c_f [mm]	8
P_t [mm]	46.1
P_l [mm]	39.9

[1]The tube bundle layout angle is defined as: $\beta = \tan^{-1}\left(\frac{P_t}{2P_l}\right)$

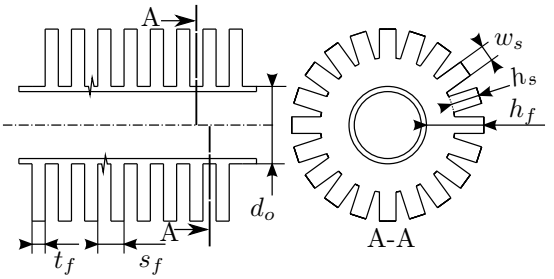

Figure 3.6: Fin tube geometric parameters

A preliminary evaluation in the present work compared the thermal-hydraulic prediction with experimental data for a fully serrated geometry (Table 3.1) using two different eddy viscosity turbulence models. Both models are capable of resolving the thermal- and velocity boundary layers, provided sufficient grid resolution, without wall function approximations.

The match with experimental data was excellent, both quantitatively and qualitatively (Figure 3.5). Moreover, the two turbulence models gave comparable results, indicating that turbulence model selection may not be critical. The latter conclusion corroborates earlier work by Nemati and Moghimi [7] who showed that several turbulence models give very similar results, except for the standard k-ε and standard k-ω models. Based on this evaluation, the Spalart-Allmaras turbulence model is selected due to its favorable convergence characteristics.

References

[1] Henk Kaarle Versteeg and Weeratunge Malalasekera. *An introduction to computational fluid dynamics: the finite volume method*. Second Edi. Pearson Education, 2007.

[2] Mi Sandar Mon and Ulrich Gross. "Numerical study of fin-spacing effects in annular-finned tube heat exchangers". In: *International Journal of Heat and Mass Transfer* 47.8-9 (2004), pp. 1953–1964. ISSN: 00179310. DOI: 10.1016/j.ijheatmasstransfer.2003.09.034.

[3] Marco Torresi et al. "CFD Analysis of the Flow Through Tube Banks of HRSG". In: *Proceedings of ASME Turbo Expo 2008, Berlin, Germany*. 2008, pp. 1–11.

[4] A. Lemouedda et al. "Numerical investigations for the optimization of serrated finned-tube heat exchangers". In: *Applied Thermal Engineering* 31.8-9 (2011), pp. 1393–1401. ISSN: 13594311. DOI: 10.1016/j.applthermaleng.2010.12.035.

[5] Cathal T. Ó Cléirigh and William J. Smith. "Can CFD accurately predict the heat-transfer and pressure-drop performance of finned-tube bundles?" In: *Applied Thermal Engineering* 73.1 (2014), pp. 681–690. ISSN: 13594311. DOI: 10.1016/j.applthermaleng.2014.08.019.

[6] E. Martinez et al. "Numerical simulation of turbulent air flow on a single isolated finned tube module with periodic boundary conditions". In: *International Journal of Thermal Sciences* 92 (2015), pp. 58–71. ISSN: 12900729. DOI: 10.1016/j.ijthermalsci.2015.01.024.

[7] Hossain Nemati and Mohammad Moghimi. "Numerical Study of Flow Over Annular-Finned Tube Heat Exchangers by Different Turbulent Models". In: *CFD Letters* 6.3 (2014).

[8] Erling Næss. "Experimental investigation of heat transfer and pressure drop in serrated-fin tube bundles with staggered tube layouts". In: *Applied Thermal Engineering* 30.13 (2010), pp. 1531–1537. ISSN: 13594311. DOI: 10.1016/j.applthermaleng.2010.02.019.

Chapter 4

Paper 1 — A validated CFD model of plain and serrated fin-tube bundles

Published in the Elsevier journal *Applied Thermal Engineering*

A validated CFD model of plain and serrated fin-tube bundles

Karl Lindqvist*, Erling Næss

Department of Energy and Process Engineering,
Norwegian University of Science and Technology, N-7491 Trondheim, Norway

Abstract

This work presents a Computational Fluid Dynamics model of helically wound fin tube bundles and demonstrates its predictive capability for thermal-hydraulic performance. A consistent validation against experimental data is given for four different fin tube geometries, two with plain fins and two with serrated fins. Predicted heat transfer and pressure drop data are within, or very close to, the experimental uncertainty, with maximum root mean square errors of 13.8 % and 14.4 % respectively. The modeled fin temperature distribution is used to evaluate three fin efficiency models, revealing that correction equations can be in significant error for tall plain fins. Three sets of semi-empirical correlations for Nusselt and Euler numbers are also evaluated, showing non-conservative predictions for several of the tested geometries. Results from the study confirm the efficacy of reduced domain modeling, whereby geometric periodicity of the heat exchanger array is exploited to reduce computational cost.

Keywords: Numerical modeling; CFD; serrated fin; plain fin; thermal-hydraulic correlations; fin efficiency

Full article at publisher: https://doi.org/10.1016/j.applthermaleng.2018.07.060

1. Introduction

Waste heat recovery is currently under consideration in the offshore oil- and gas industry to mitigate the high energy use on platforms. Weight- and volume minimization of the heat exchanger core is vital due to the lack of space on these installations. Earlier work has indicated that overall Waste Heat Recovery Unit (WHRU) skid weight can be reduced by bringing down the tube diameter [1], which calls for an extension of the validity range of existing thermal-hydraulic design correlations. It is also highly desirable to be able to validate the performance of a thermally optimized design by detailed numerical modeling, before investing in fabrication and experimental testing. Computational Fluid Dynamics (CFD) can supplement experimental measurements and provide additional insights in this endeavor, provided that models are thoroughly validated.

Numerical CFD models have thus far contributed both qualitatively and quantitatively to the thermal-hydraulic modeling of finned tubes. Qualitatively, by giving an understanding the local flow phenomena around finned tubes. Quantitatively, by enabling sensitivity studies which are very time consuming to study experimentally.

As will be shown in the following, the majority of earlier modeling efforts have focused on simulating plain fin tubes, tube bundles with few (<5) tube rows and/or annular fin tubes. Large diameter tubes (≥25.4 mm) have been prioritized. Industrial relevance, combined with the possibility to exploit geometrical symmetry while keeping model size moderate have likely been the reasons behind this focus. In contrast, compact offshore waste heat recovery units can be expected to use helically wound serrated fins with small diameter tubes [2]. Moreover, many studies have compared modeling results with empirical correlations as a means of model validation. This approach is insufficient if model data are to be treated on par with experimental data, due to the large spread in

*Corresponding author
Email address: karl.erik.lindqvist@ntnu.no (Karl Lindqvist)

predictions between different correlations.

The dissertation by Mon [3] constitute one of the first application of CFD to finned tube bundles. 29 different tube bundles with plain annular fins were modeled in staggered and in-line configuration, all having four tube rows. Mon's CFD model was capable of describing intuitive, qualitative trends in overall heat transfer performance. The simulations were used to propose a correction to the VDI Heat Atlas correlation [4], although direct validation with experiments were lacking. In a consecutive paper, Mon and Gross [5] compared results for eight of the modeled tube bundles to a few literature correlations. Similar work has been presented in [6, 7, 8], of which only Pathak et al. compared modeling results with experimental data.

The research by McIlwain [9] has many similarities with the work of Mon. Qualitative flow features were used to improve the pressure loss coefficients in the HTFS2 correlation. Six tube rows were modeled in all cases and plain annular fins were considered. Experimental data for four in-line tube bundles and one staggered tube bundle was used for model validation, with good, albeit somewhat inconsistent, results.

Torresi et al. [10] modeled the pressure drop over a single serrated finned tube row and subsequently implemented a porous region model for the analysis of a full Heat Recovery Steam Generator (HRSG). Benchmark results compared favorably to a corresponding simulation in a proprietary 1D pressure loss code, but no comparison with experiments were made.

McIlwain [11] simulated two different single row tube bundles with plain and serrated fins, respectively, in order to explain the higher pressure drop and heat transfer rate of serrated fins. The same author also simulated a serrated fin-tube in multi-row inline configurations and compared the resulting pressure drop to that predicted from an industrial correlation [12].

The thesis of Hofmann [13] and subsequent publications [14, 15] presented experimental measurements and numerical models of one plain- and two serrated fin-tube geometries. Modeled and measured Nusselt numbers and pressure drop coefficients matched with reasonable accuracy, but significant scatter was seen in the experimental data. Only one tube row was modeled numerically. A particular model simplification was evaluated and concluded to be acceptable, namely to model helically wound fins as annular (flat) fins. It should, however, be noted that the investigated geometries had a relatively low fin pitch, making them amenable to this simplification.

Lemouedda et al. [16] compared the heat transfer/ pressure drop trade-off of plain versus serrated fins in a three-row tube bundle and studied the effect of fin tip twist and the number of fin segments. The study only considered moderate Reynolds numbers ($1320 \leq Re_{d_o} \leq 5750$) and did not validate the model with experiments. Moreover, it is the only published study, to the authors knowledge, that neglect turbulence modeling altogether and assume laminar flow.

Ó Cléirigh and Smith [17] modeled the heat transfer and pressure drop of three finned tube geometries with varying degree of serration (from plain, through halfway serrated to fully serrated). They showed that CFD gives similar results as correlations over large range of Reynolds numbers. Neither this study showed validation with experiments.

Martinez et al. [18] presented a modeling approach where a small section of a finned tube bank is simulated with fully periodic boundary conditions. Nusselt numbers and friction factors were compared with two correlations with satisfactory agreement. Detailed flow field data were also compared to experimental measurements. The authors went on to perform similar modeling of a six-row tube bundle including inlet and outlet regions in a subsequent publication [19]. A major conclusion of this work was that velocity, temperature and turbulence fields indeed show periodic behavior after the third tube row and that a fully periodic model therefore is appropriate. The same six-row setup was finally used to show that a relatively large part of the fin can be removed without significantly affecting thermal-hydraulic performance [20].

In summary, only one publication (namely [9]) has validated simulations of more than one tube geometry, using a consistent numerical setup, with experimental data. This is troublesome, since an insufficient numerical setup or grid generation technique may seem acceptable for one particular geometry but break down in the general case. The validation case therefore needs to be revisited for helically wound fin tubes in staggered tube configurations, particularly for serrated fins. On a technical note, all but one publication make use of Reynolds averaging coupled with an eddy viscosity model of either k-ϵ or k-ω type. Due to the lack of validation, it is not clear at this point whether this modeling approach is sufficient or if higher fidelity modeling is needed.

The novelty of this study is firstly that the numerical model's predictive capabilities are demonstrated

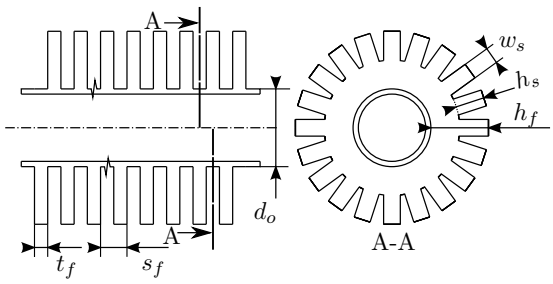

Figure 1: Fin tube geometric parameters

Table 1: Tube and array geometries (cf. Figure 1 and Figure 2). All dimensions in mm unless stated.

Geometry	A	B	C	D
Reference	[21]	[22]	[23]	[24]
Fin type	plain	plain	serrated	serrated
Fin material	aluminum	copper	steel	steel
d_o [mm]	13.5	15.9	20.87	50.8
h_f [mm]	10	1.42	8.61	25.78
h_s [mm]			8.61	20.83
t_f [mm]	0.5	0.41	0.91	1.22
s_f [mm]	2.81	1.3	5.08	4.28
w_s [mm]			3.97	4.32
β^1 [deg]	30	30	30	30
c_f [mm]	5.2	8.8	8	11.94
P_t [mm]	38.7	27.5	46.1	114.3
P_l [mm]	33.5	23.9	39.9	99.0
h_f/r_o [-]	1.48	0.18	0.83	1.01
$h_f/\hat{s}_f$ [-]	4.33	1.60	2.06	8.42

[1]The tube bundle layout angle is defined as

$$\beta = \tan^{-1}\left(\frac{P_t}{2P_l}\right)$$

over a large range of tube- and fin dimensions. Consistent validation against experimental data for four rather different fin tube geometries from the literature is given. Secondly, the paper aims to evaluate the accuracy of fin efficiency correction equations, particularly for small diameter and high finned tubes. Fin efficiency corrections have received comparatively little attention in the literature, but can influence performance predictions significantly for non-standard fin tube geometries. A few selected thermal-hydraulic correlations are also discussed. The modeling approach and methods used in this paper are generally applicable for thermal-hydraulic performance estimation, particularly for heat exchangers with stream- and spanwise periodic geometry.

2. Fin tube geometries and semi-empirical equations

Four finned tube geometries from the literature are modeled in the present work, with geometric parameters given in Table 1 and depicted schematically in Figure 1. All geometries have previously been tested experimentally in multi-row staggered configurations in dedicated wind tunnels that are expected to be representative of conditions in a WHRU. Three sets of thermal-hydraulic correlations are used for reference, namely the mathematically simple PFR correlations [25], the industrially popular ESCOA correlations [26] and the recent correlations by Holfeld [21]. Relatively small diameter tubes are chosen to explicitly violate the validity ranges of the PFR and ESCOA correlations.

A measure of the uncertainty of the experimental data is necessary for a correct comparison with results from numerical modeling. Holfeld [21] reported uncertainties of 9.0–16.7 % for the Nusselt number and 25.2–4.3 % for the Euler number. The range corresponds to uncertainties at low Re and high Re, respectively. Næss [23] reported uncertainties of 4–8 % for Nusselt numbers and 10–2 % for Euler numbers. Since uncertainty analyses are missing in [24] and [22], we assume an approximate measurement uncertainty of 10 % for heat transfer and 15 % for pressure drop based on a review of other sources and taking all uncertainties (measured quantities, geometry, production standards, tube inside heat transfer) into account. These numbers also reflect the additional uncertainty in the Reynolds number.

Two correlations for fin efficiency correction are considered in this work, namely the Weierman correction [27],

$$\frac{\eta_f}{\eta_{f,\text{theo}}} = \begin{cases} 0.7 + 0.3\eta_{f,\text{theo}} & \text{Plain fin} \\ 0.9 + 0.1\eta_{f,\text{theo}} & \text{Serrated fin} \end{cases}$$

and the Hashizume correction [28],

$$\frac{\eta_f}{\eta_{f,\text{theo}}} = 1 - (mh_f) \cdot \left(a + 0.14\left(\frac{d_o + 2h_f}{d_o}\right)^{2.7}\left(1 - 0.097\ln(\text{Re}_{d_o})\right)\right)$$

with

$$a = \begin{cases} 0 & \text{Plain fin} \\ 0.016\left(\frac{h_s}{w_s}\right) & \text{Serrated fin} \end{cases}$$

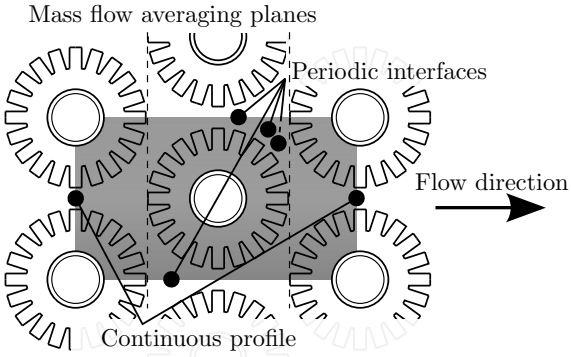

Figure 3: Reduced domain model setup

The theoretical fin efficiency is calculated based on the work of Hashizume et al. [28].

3. Numerical model

The numerical modeling approach in this paper is based on simulating a periodic "unit cell" in the heat exchanger array, building on the work of Martinez et al. [18] (cf. Figure 3). This approach reduces the computational cost considerably over modeling a full tube bundle. One of the tube geometries is also modeled in an eight row configuration (cf. Figure 2) to verify the efficacy of the reduced domain model. The common modeling assumptions are given in the following paragraphs.

3.1. Model equations and numerical setup

The steady Reynolds Averaged Navier-Stokes (RANS) equations are solved together with the energy equation and a model equation for turbulence using the open source CFD toolbox OpenFOAM v4.1. Second order upwind discretization is used for all convective terms. The Spalart-Allmaras turbulence model is selected due to its simplicity, robustness and suitability for simulating boundary layers under adverse pressure gradient conditions. It also yields similar results as other eddy viscosity turbulence models when applied to finned tube bundles [29]. All model constants were kept at their default value.

Turbulent viscosity is set to zero on solid wall surfaces, except for the fin tip and segment sides where wall functions for turbulent viscosity and turbulent thermal diffusivity are used. A turbulent Prandtl number of 0.85 is used throughout for thermal diffusivity calculations. The tube surface and the fin root is given a fixed temperature boundary condition of 298 K. Fin surfaces exposed to the fluid uses a coupled boundary condition with a consistent heat flux across the interface.

Two iterative convergence criteria are used: The drop in mass averaged total pressure ($p_0 + 0.5\rho U^2$) across the computational domain and the total surface heat flux from each fin surface. Equation residuals were also checked for monotonic reduction.

3.2. Thermophysical models

The fluid is modeled as dry air with constant thermophysical properties, including density. This simplification removes the dependency on whether the gas is cooled or heated by the tubes and is justified by the fact that the gas temperature change for each tube row usually is moderate. Even if it is not, the impact on the heat transfer coefficient should be negligible for gas cooling (heat recovery) applications as long as boundary layers remain laminar [30]. As regards the pressure drop, it is common practice to perform measurements in separate, adiabatic, experiments. Hence, the numerical simulations are representative of the experimental setup in this regard. Some thermal-hydraulic correlations indeed correct for the direction of heat flow, but to verify such dependencies is outside the scope of this paper.

The fins are modeled using an isotropic conducting material with constant thermal conductivity corresponding to carbon steel ($48.5\,\mathrm{W\,m^{-1}\,K^{-1}}$), aluminum ($193\,\mathrm{W\,m^{-1}\,K^{-1}}$) or copper ($375\,\mathrm{W\,m^{-1}\,K^{-1}}$), matching the experimental setup.

3.3. Full tube bundle model

The computational domain and boundary conditions for the full tube bundle model are indicated schematically in Figure 2. A single fin pitch is modeled in the spanwise direction (not shown), using periodic boundary conditions, following [17]. A uniform profile for velocity, temperature and modified turbulent viscosity is prescribed on the inlet, with a Neumann condition for pressure. Conversely, pressure in prescribed on the domain outlet.

3.4. Reduced domain model

The reduced domain (depicted in Figure 3) uses a prescribed velocity profile on the leftmost ("inflow") boundary and a prescribed pressure profile on the

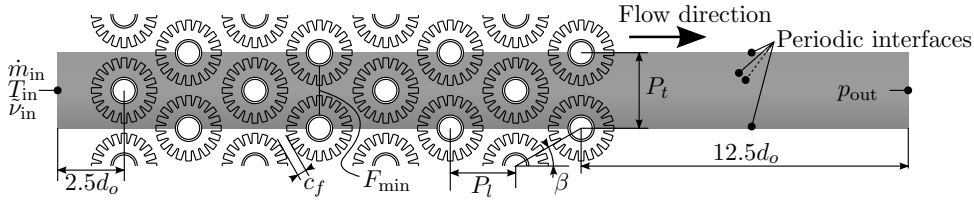

Figure 2: Computational domain, boundary conditions and array parameters; Full domain model

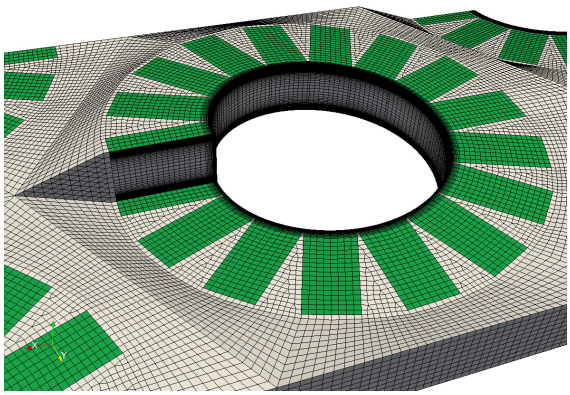

Figure 4: Computational grid example; Fully serrated fin, fin domain colored green, bulk fluid cell size is enlarged for clarity

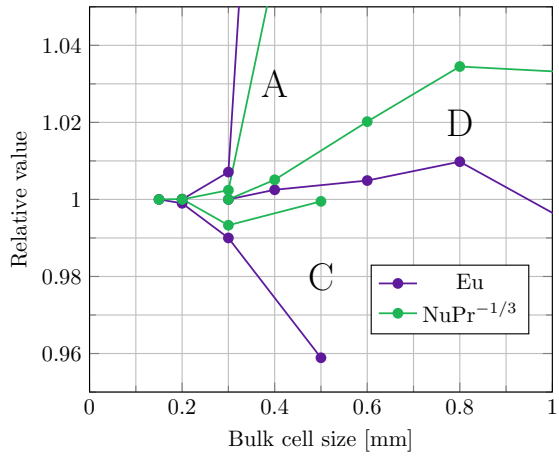

Figure 5: Grid convergence for fin-tube geometries A, C and D

rightmost ("outflow") boundary, with Neumann conditions for pressure and velocity, respectively. The profiles are updated regularly during the solution process by sampling from the opposing patch, in a staggered fashion, to avoid numerical instability. The profiles for temperature and modified turbulent viscosity are updated every iteration, acting as a fully periodic boundary. Uniform profiles are used initially. The number of iterations between profile updates are adjusted to ensure convergence. In addition to being copied, profiles for velocity and temperature are scaled to satisfy a specified area average, such that flow rate and temperature difference can be set. Simulations are considered converged when total pressure drop and surface heat fluxes does not change significantly between profile updates, nor with continued iterations.

3.5. Grid generation and grid convergence study

A hexahedra-dominated hybrid grid is generated around the fin-tubes consisting of a boundary-layer resolving grid in the fluid gap between the fins and an approximately uniform grid for the bulk fluid between the fin tubes. Polyhedral cells are used to connect the two mesh regions. This ensures a consistent resolution of the inter-fin flow, with $y^+ < 1$ and a sufficient number of cells in the boundary layer, for all bulk fluid cell sizes. A typical computational grid is shown in Figure 4. The asymmetric geometry of the helically wound fin is accurately represented, which is believed to be important for an accurate pressure drop prediction.

Grid convergence is tested on the reduced computational domain for three of the fin-tube geometries (A, C and D). The bulk fluid resolution is varied while keeping the boundary layer growth rate and wall y^+ constant. Euler and Nusselt numbers are generally found to be within $\pm 1\,\%$ of its asymptotic value at a bulk cell size of 0.3 mm, as shown in Figure 5. A cell size of 0.4 mm is judged acceptable for the largest fin-tube, but it is interesting to note that the resolution requirement does not scale with the tube or fin dimensions. The boundary layer growth rate was varied independently for one of the tube geometries as an additional test. Comparing simulations with a 7 % growth and a 20 % growth rate revealed differences in Euler and Nusselt numbers of less than

0.1 %. Hence, a boundary layer cell growth rate of 20 % was used throughout for production simulations. Adiabatic boundary conditions were used for fin tips and segment sides in the grid convergence tests.

4. Data reduction

Upon convergence, the raw data from the numerical model (T,p,U,... fields) is integrated and reduced to Nusselt, Euler and Reynolds numbers to facilitate interpretation and comparison with correlations. *Average* Nusselt and Euler numbers are calculated for the full tube bundle simulation, whereas local numbers are calculated for the single central tube in the reduced domain case.

The temperature and pressure fields of the fluid are mass flow averaged before and after the fin-tube bundle as a basis for the data reduction. The inflow and outflow boundaries are used for this purpose in the full domain case. For the reduced domain, mass flow averaging planes are inserted before and after the central fin-tube, as indicated in Figure 3, to compute the drop in total pressure ($p_0 + 1/2\rho U^2$). Mass flow averaging planes are also inserted in the full domain model for comparison with the data reduction of the reduced domain model.

The wall heat flux from the active heat transfer area is evaluated numerically based on Fourier's law and the near-wall fluid temperature gradient. The bulk temperatures used in heat flux normalization are then computed from the inlet temperature plus the per-row temperature change to ensure consistency, viz.

$$T_{b,i} = T_{b,\text{in}} + \frac{\sum_{n=1}^{n=i-1} \dot{Q}_{w,n}}{\dot{m} c_{p,m}} \tag{1}$$

for tube row index $i \in \{1, \ldots, N_r + 1\}$. For reduced domain cases, $T_{b,\text{in}}$ is the bulk temperature on the periodic inlet.

The heat transfer coefficient is calculated as

$$\alpha_o = \frac{\dot{Q}_f + \dot{Q}_t}{[\eta_f A_f + A_t]\Delta T} \tag{2}$$

where, in the full tube bundle simulation, η_f is the area average fin efficiency and ΔT is the log mean temperature difference,

$$\Delta T = \frac{(T_{b,\text{in}} - T_t) - (T_{b,\text{out}} - T_t)}{\ln(T_{b,\text{in}} - T_t) - \ln(T_{b,\text{out}} - T_t)} \tag{3}$$

The reduced domain cases uses the arithmetic temperature difference (since no counter-flow occurs in a single tube row),

$$\Delta T \approx \Delta T_\text{A} = \frac{1}{2}((T_{b,\text{before}} - T_t) + (T_{b,\text{after}} - T_t)) \tag{4}$$

where $T_{b,\text{before}}$ and $T_{b,\text{after}}$ are bulk temperatures before and after the central tube, respectively.

The fin efficiency is evaluated from the computed fin surface temperature field,

$$\eta_f = \frac{\dot{Q}_\text{actual}}{\dot{Q}_\text{ideal}} = \frac{\alpha_o \int_\text{fin} (T_b - T_f)\,\text{dA}}{\alpha_o A_f (T_b - T_t)} = \frac{T_b - T_{f,\text{avg}}}{T_b - T_t} \tag{5}$$

where $T_{f,\text{avg}}$ is the area-averaged temperature of the fin, viz.

$$T_{f,\text{avg}} = \frac{1}{A_f} \int_\text{fin} T_f \,\text{dA} \tag{6}$$

The heat transfer coefficient is normalized by the outer diameter of the tubes, and the fluid properties, forming

$$\text{NuPr}^{-1/3} = \frac{d_o \alpha_o}{k} \left(\frac{c_p \mu}{k}\right)^{-1/3} \tag{7}$$

The Reynolds number is correspondingly defined as

$$\text{Re} = \frac{d_o u_{F_\text{min}}}{\nu} \tag{8}$$

The pressure drop is normalized by the velocity head in the minimum free flow area $\frac{1}{2}\rho u^2_{F_\text{min}}$, viz

$$\text{Eu} = \frac{\Delta p}{\frac{1}{2}\rho u^2_{F_{min}} N} = \frac{\rho \Delta p}{\frac{1}{2}\dot{m}'^2 N} \tag{9}$$

where N is the number of tube rows that Δp is calculated over.

Finally, the theoretical and corrected fin efficiencies are needed for later comparison with the numerically integrated one (Equation 5). An iterative method is needed to find the theoretical, and the corrected theoretical, fin efficiency from the raw simulation data (Q_f, Q_t, A_f, A_t, ΔT). This is a result of the implicit equation for the outer heat transfer coefficient:

$$\alpha_o = \frac{\dot{Q}_f + \dot{Q}_t}{[\eta_{f,\text{theo}}(\alpha_o, d_o, h_f, \ldots) A_f + A_t]\,\Delta T} \tag{10}$$

This equation can be solved by back-substitution, i.e. by guessing an outer heat transfer coefficient, calculating the fin efficiency, and then updating α_o and

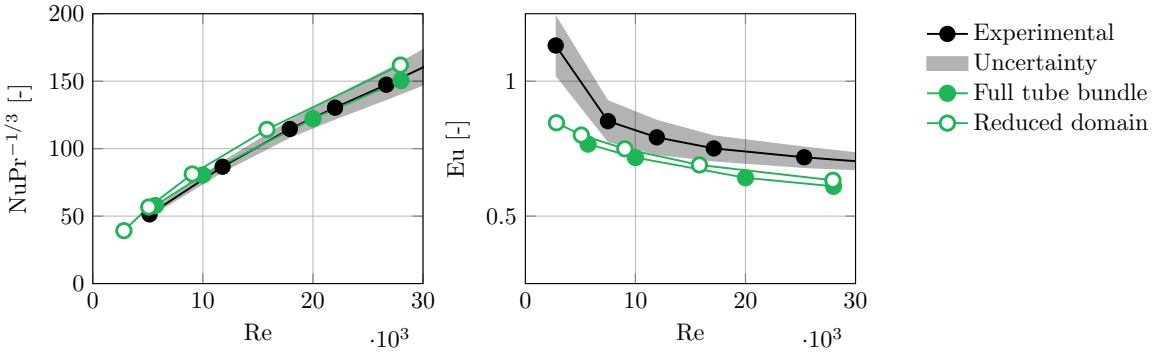

Figure 6: Full versus reduced domain, geometry C

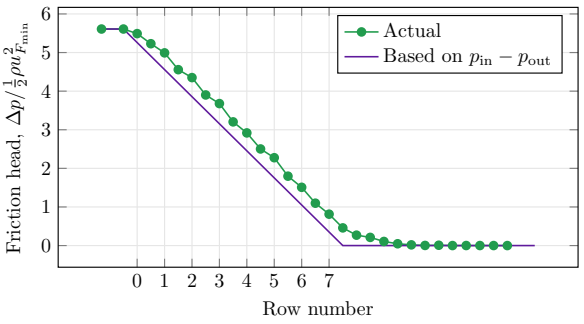

Figure 7: Mass averaged pressure change through the full tube bundle model

η_f in succession until convergence. Note, therefore, that each method of calculating η_f corresponds to a unique α_o, since the transferred heat and ΔT remain constant.

5. Results and discussion

5.1. Full domain versus reduced domain model

Figure 6 shows a comparison between the Nusselt and Euler numbers of the full tube bundle model, the reduced domain model and experimental data for tube bundle C. It is clear that the reduced domain model gives near identical results compared to the full tube bundle model, at a much reduced computational cost. The small differences between the models can be attributed to the different expressions for ΔT used in data reduction as well as tube bundle entry and exit effects.

Figure 7 shows the pressure profile in the full tube bundle model, including entry and exit effects. The slope of the actual pressure curve, taken between two points spaced one tube row apart, matches well with the average pressure curve after the first tube row. This confirms earlier indications that the reduced model is representative of the full tube model after (at least) the third tube row [18] and that a data reduction method using mass averaged pressure planes to compute the Euler number is acceptable.

The computational cost for the reduced domain model was approximately one-seventh of that of the full domain model, which reflects the difference in the physical size of the domain as well as the faster convergence of the reduced model. The differences in model sizes and solution times for all cases are shown in Table 2.

5.2. Predictive accuracy of CFD

Nusselt and Euler numbers predicted by the reduced domain numerical model are compared to experimental data and reference correlations in Figures 8 to 11. In general, numerical model predictions are either within or close to the experimental uncertainty region of all four fin-tube geometries. The largest root mean square errors are 13.8 % for heat transfer (Geometry A) and 14.4 % for pressure drop (Geometry

Table 2: Grid size and computational cost comparison; all simulations performed on a compute cluster based on Intel Xeon E5-2670 processors

Geometry	A	B	C		D
Modeled domain	reduced	reduced	full	reduced	reduced
Inter-tube cell size [mm]	0.20	0.20	0.20	0.20	0.40
Fluid domain cell count [$\cdot 10^6$]	4.21	1.28	15.36	3.70	5.68
Solution time [CPU-hr]	331	136	2355	327	148

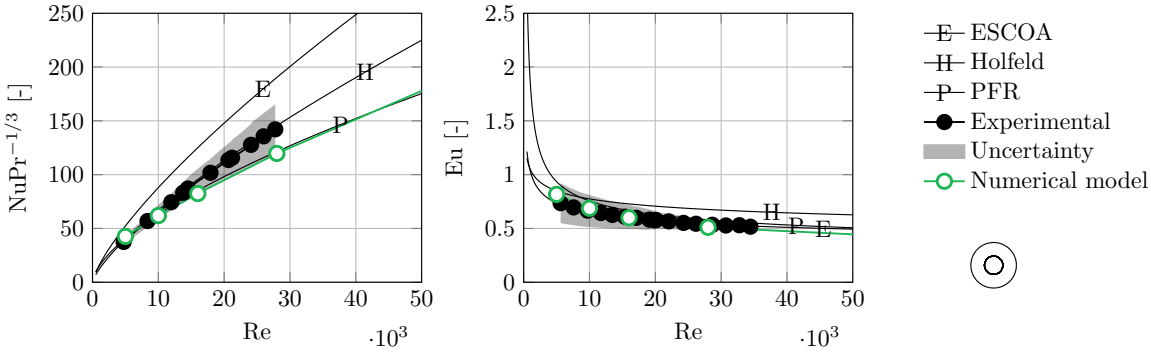

Figure 8: Thermal-hydraulic results, Geometry A; Experimental data and uncertainty from [21]

C). These errors are likely the result of inaccurate geometric representation (e.g. failure to model segment fin tip twist, burr edges and weld fillets) and/or turbulence model errors. No major difference can be seen in the prediction accuracy of plan fins versus that of serrated fins. This is encouraging, given the more complex flow around serrated fins, with repetitive boundary layer breakup and fluid mixing.

5.3. Thermal-hydraulic correlation accuracy

A few interesting trends can be noted regarding the predictive accuracy of the selected thermal-hydraulic correlations. The Holfeld correlations are clearly the superior equation set for predicting heat transfer for the investigated geometries. The ESCOA correlations for heat transfer perform poorly for the three small-diameter geometries, with errors of around 50 %. The PFR correlations perform relatively well given their simplicity, but relatively large errors are seen for geometry C. Notably, the three heat transfer correlations agree well for the large diameter tube.

The pressure drop predictions show a different trend than the heat transfer predictions. Overall, the PFR correlation gives best predictions, with the Holfeld correlations being moderately more in error for geometry B. The ESCOA correlations again err significantly or the non-conservative side, particularly for the serrated fin tubes. The three pressure drop correlation sets agree more for the small diameter tubes compared to the large diameter one.

5.4. Fin efficiency correction accuracy

Figure 12 shows a comparison between the numerically integrated fin efficiency and the two selected fin efficiency correction equations. For geometry A, the actual (numerical) fin efficiency is quite close to the theoretical one ($\eta_f/\eta_{f,\text{theo}} = 1$), even at high Reynolds numbers, indicating that a correction is largely unnecessary. The two proposed correction equations are indeed further away from the numerically integrated one, and hence detract from modeling accuracy. The unusual ratio between fin height and tube diameter of geometry A can explain this discrepancy.

Contrary to geometry A, the actual fin efficiency of geometry C and D is substantially lower than what the theoretical fin efficiency model predicts. The Weierman correction offers significant improvement over the theoretical model, although an even stronger correction would be needed in these cases to fully compensate for the non-uniform heat transfer coefficient.

The Hashizume correction degrades accuracy for all considered cases, and indeed has a slope inconsis-

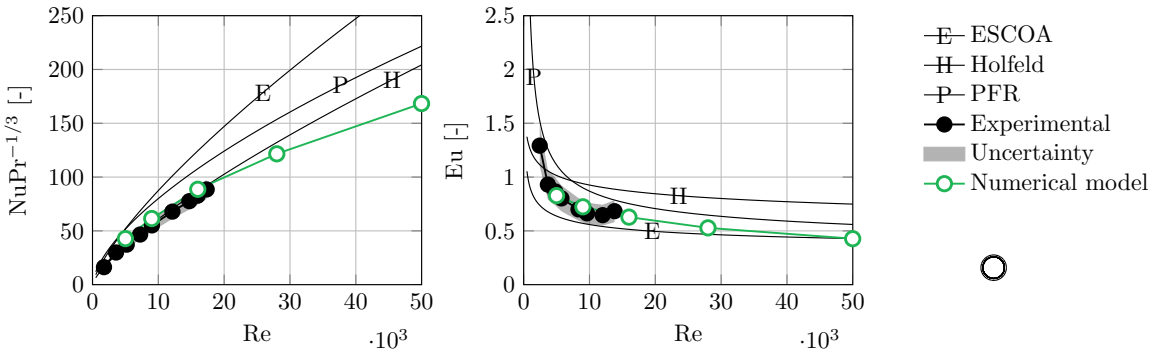

Figure 9: Thermal-hydraulic results, Geometry B; Experimental data from [22], estimated uncertainty

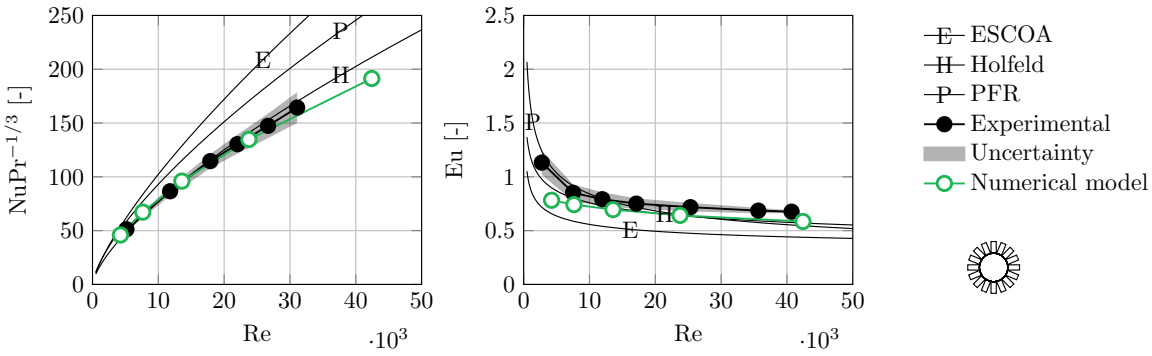

Figure 10: Thermal-hydraulic results, Geometry C; Experimental data and uncertainty from [23]

tent with the data from the numerical models. In fairness, it should be noted that all three geometries violate the validity ranges of the Hashizume equation slightly, but the correction nonetheless appear excessively strong.

6. Conclusions

This paper has presented a numerical model of solid and serrated fin-tube bundles, compared results to experimental data as well as semi-empirical correlations and used the numerically calculated fin temperature distribution to evaluate fin efficiency models. The following conclusions are drawn:

- RANS-based simulations can predict the thermal-hydraulic performance of fin-tube bundles with good accuracy for a range of helically wound solid- and serrated-fin geometries, provided that best practice grid generation guidelines are followed and that grid convergence is demonstrated
- Numerical simulations enable time efficient and consistent parameter studies, particularly when geometric periodicity can be exploited
- Compared to empirical correlations, the heat transfer results are consistent with the recent Holfeld correlation for the selected geometries. There is considerable inconsistencies between the correlations for pressure drop, and no single correlation capture the numerical predictions for all geometries.
- Access to the local fin temperature distribution enables fin efficiency evaluations which would have been quite tedious to perform experimentally.
- In general, the fin efficiency, calculated on the basis of a constant heat transfer coefficient, is negatively influenced by the actual uneven heat transfer coefficient distribution. The reduction in fin efficiency depends on the fin geometry and material, and the magnitude of the average

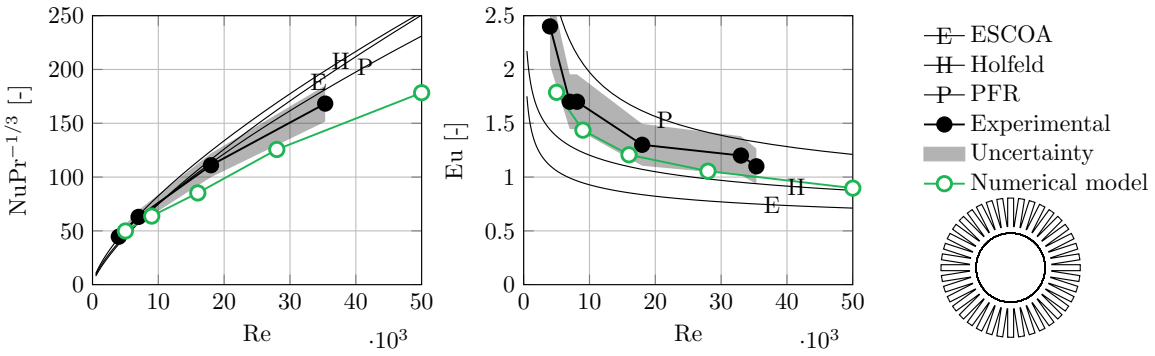

Figure 11: Thermal-hydraulic results, Geometry D; Experimental data from [24], estimated uncertainty

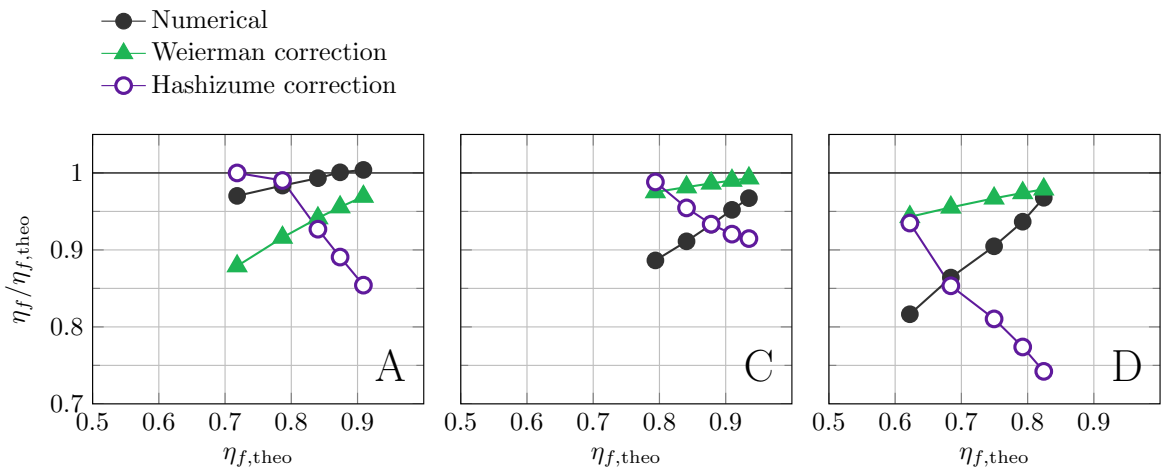

Figure 12: Fin efficiency correction equations compared to exact fin efficiency from numerical simulations for fin-tube geometries A, C and D.

heat transfer coefficient. The fin-correction correlation of Weierman captures the numerically computed trends, but does not reproduce the numerical values. Clearly, more work is required in this area.

Numerical simulations are well suited to perform broader parameter studies in future work, in order to identify the exact applicability limits of current correlations and suggest areas where further experimental work is needed. Simulations will also continue to have an important role in the heat exchanger design process, in addition to correlations and experimental validation.

Acknowledgment

The authors acknowledge the partners: Neptune Energy Norge AS, Alfa Laval, Statoil, Marine Aluminium, NTNU, SINTEF and the Research Council of Norway, strategic Norwegian research program PETROMAKS2 (#233947) for their support.

Nomenclature

A_f	fin heat transfer area [m^2]
A_t	tube heat transfer area [m^2]
d_o	outer tube diameter [m]
$F_{\min}$	minimum free flow area [m^2]
h_f	total fin height [m]
h_s	segmented height [m]
m	nondimensional fin parameter [-]
$\dot{m}$	mass flow [$kg\,s^{-1}$]
$\dot{m}''$	mass flux ($= \dot{m}/F_{\min}$) [$kg\,s^{-1}\,m^{-2}$]
N	number of tube rows [-]
p	total pressure [Pa]
p_0	static pressure [Pa]
P_t	transverse tube pitch [m]
P_l	longitudinal tube pitch [m]
$\dot{Q}$	heat flow [W]
s_f	fin pitch [m]
$\hat{s}_f$	fin aperture ($= s_f - t_f$) [m]
T	temperature [K]
t_f	fin thickness [m]
$u_{F_{min}}$	mean velocity in minimum free flow area [$m\,s^{-1}$]
w_s	segment width [m]
y^+	nondimensional wall distance [-]

Greek symbols

α_o	external heat transfer coefficient [$W\,m^{-2}\,K^{-1}$]
α_e	apparent heat transfer coefficient [$W\,m^{-2}\,K^{-1}$]
β	tube bundle layout angle [°]
η_f	fin efficiency [-]
$\tilde{\nu}$	modified turbulent viscosity [$m^2\,s^{-1}$]

Subscripts

avg	average
b	bulk, mixing cup
f	fin
t	tube
theo	theoretical

References

[1] G. Skaugen, H. T. Walnum, B. A. L. Hagen, D. P. Clos, M. Mazzetti, P. Nekså, Design and optimization of waste heat recovery unit using carbon dioxide as cooling fluid, in: Proceedings of the ASME 2014 Power Conference, 2014, pp. 1–10.

[2] A. Holfeld, E. Næss, Influence of the Fin Type and Base Tube Diameter of Serrated and Solid-Fin Tubes on the Heat Transfer and Pressure Drop Performance, in: Proceedings of the 15th International Heat Transfer Conference, IHTC-15, 1, Tokyo, Japan, 2014, pp. 1–12.

[3] M. S. Mon, Numerical investigation of air-side heat transfer and pressure drop in circular finned-tube heat exchangers, Ph.D. thesis, Technischen Universität Bergakademie Freiberg, 2003.

[4] P. Stephan, S. Kabelac, M. Kind, H. Martin, D. Mewes, K. Schaber, VDI Heat Atlas, Springer Berlin Heidelberg, Berlin, Heidelberg, 2010.

[5] M. S. Mon, U. Gross, Numerical study of fin-spacing effects in annular-finned tube heat exchangers, International Journal of Heat and Mass Transfer 47 (2004) 1953–1964.

[6] R. K. Banerjee, M. Karve, J. H. Ha, D. H. Lee, Y. I. Cho, Evaluation of Enhanced Heat Transfer Within a Four Row Finned Tube Array of an Air Cooled Steam Condenser, Numerical Heat Transfer, Part A: Applications 61 (2012) 735–753.

[7] H. Bilirgen, S. Dunbar, E. K. Levy, Numerical modeling of finned heat exchangers, Applied Thermal Engineering 61 (2013) 278–288.

[8] S. Pathak, K. Velusamy, K. Rajan, C. Balaji, Numerical and experimental investigations of heat removal performance of sodium-to-air heat exchanger used in fast reactors, Heat Transfer Engineering 36 (2015) 439–451.

[9] S. R. McIlwain, Improved Prediction Methods for Finned Tube Bundle Heat Exchangers in Crossflow, Ph.D. thesis, University of Strathclyde, 2003.

[10] M. Torresi, A. Saponaro, S. M. Camporeale, B. Fortunato, CFD Analysis of the Flow Through Tube Banks of HRSG, in: Proceedings of ASME Turbo Expo 2008, Berlin, Germany, 2008, pp. 1–11.

[11] S. R. McIlwain, A Comparison of Heat Transfer Around a Single Serrated Finned Tube and a Plain Finned Tube, International Journal of Research & Reviews in Applied Sciences 2 (2010) 88–94.

[12] S. R. McIlwain, A CFD Comparison of Heat Transfer and Pressure Drop Across Inline Arrangement Serrated Finned Tube Heat Exchangers With an Increasing Number of Rows, International Journal of Research & Reviews in Applied Sciences 4 (2010) 162–169.

[13] R. Hofmann, Experimental and Numerical Air-Side Performance Evaluation of Finned-Tube Heat Exchangers, Ph.D. thesis, Technischen Universität Wien, 2009.

[14] R. Hofmann, H. Walter, Experimental and Numerical Investigation of the Gas Side Heat Transfer and Pressure Drop of Finned TubesPart I: Experimental Analysis, Journal of Thermal Science and Engineering Applications 4 (2012) 041007.

[15] R. Hofmann, H. Walter, Experimental and Numerical Investigation of the Gas Side Heat Transfer and Pressure Drop of Finned TubesPart II: Numerical Analysis, Journal of Thermal Science and Engineering Applications 4 (2012) 041008.

[16] A. Lemouedda, A. Schmid, E. Franz, M. Breuer, A. Delgado, Numerical investigations for the optimization of serrated finned-tube heat exchangers, Applied Thermal Engineering 31 (2011) 1393–1401.

[17] C. T. Ó Cléirigh, W. J. Smith, Can CFD accurately predict the heat-transfer and pressure-drop performance of finned-tube bundles?, Applied Thermal Engineering 73 (2014) 681–690.

[18] E. Martinez, W. Vicente, M. Salinas-Vazquez, I. Carvajal, M. Alvarez, Numerical simulation of turbulent air flow on a single isolated finned tube module with periodic boundary conditions, International Journal of Thermal Sciences 92 (2015) 58–71.

[19] E. Martinez-Espinosa, W. Vicente, M. Salinas-Vazquez, I. Carvajal-Mariscal, Numerical Analysis of Turbulent

Flow in a Small Helically Segmented Finned Tube Bank, Heat Transfer Engineering 38 (2017) 47–62.

[20] E. Martinez-Espinosa, W. Vicente, M. Salinas-Vazquez, Numerical Analysis for Saving Fin Material in Helical Segmented-Tubes, Applied Thermal Engineering 110 (2017) 306–317.

[21] A. Holfeld, Experimental investigation of heat transfer and pressure drop in compact waste heat recovery units, Ph.D. thesis, Norwegian University of Science and Technology, 2016.

[22] D. J. Ward, E. H. Young, Heat transfer and pressure drop of air in forced convection across triangular pitch banks of finned tubes, Chem. Eng. Progr. 55 (1959).

[23] E. Næss, Experimental investigation of heat transfer and pressure drop in serrated-fin tube bundles with staggered tube layouts, Applied Thermal Engineering 30 (2010) 1531–1537.

[24] C. Weierman, J. Taborek, W. J. Marner, Comparison of the Performance of In-line and Staggered Banks of Tubes With Segmented Fins, AlChE Symposium Series 74 (1978) 39–46.

[25] PFR Engineering Systems Inc., Heat Transfer and Pressure Drop Characteristics of Dry Tower Extended Surfaces, Technical Report, PFR Report BNWL-PFR-7-100, 1976.

[26] ESCOA Fintube Corp., ESCOA Engineering Manual (electronic version), Technical Report, Downloaded September 2005 from http://www.fintubetech.com/escoa/, 2002.

[27] C. Weierman, Correlations ease the selection of finned tubes, Oil Gas J 74 (1976) 10–94.

[28] K. Hashizume, R. Morikawa, T. Koyama, T. Matsue, Fin Efficiency of Serrated Fins, Heat Transfer Engineering 23 (2002) 6–14.

[29] H. Nemati, M. Moghimi, Numerical Study of Flow Over Annular-Finned Tube Heat Exchangers by Different Turbulent Models, CFD Letters 6 (2014).

[30] W. M. Kays, M. E. Crawford, B. Weigand, Convective Heat and Mass Transfer, fourth edi ed., McGraw-Hill Education, New York, 2005.

Chapter 5

Paper 2 — On correction factors in thermal-hydraulic correlations for compact fin-tube bundles

Submitted to the Springer journal *Heat and Mass Transfer*

This paper is awating publication and is not included in NTNU Open

Chapter 6

Paper 3 — A machine learning approach to correlation development applied to fin-tube bundle heat exchangers

Published in *Energies*, an MDPI Open Access journal. The supplementary material for this article is given in the appendix.

energies

MDPI

Article

A Machine Learning Approach to Correlation Development Applied to Fin-Tube Bundle Heat Exchangers

Karl Lindqvist [1,*], Zachary T. Wilson [2], Erling Næss [1] and Nikolaos V. Sahinidis [2]

[1] Department of Energy and Process Engineering, Norwegian University of Science and Technology, NO-7491 Trondheim, Norway; erling.nass@ntnu.no

[2] Department of Chemical Engineering, Carnegie Mellon University, Pittsburg, PA 15213, USA; ztw@andrew.cmu.edu (Z.W.); niksah@gmail.com (N.V.S.)

* Correspondence: karl.erik.lindqvist@ntnu.no; Tel.: +4796829629

Received: 18 October 2018; Accepted: 06 December 2018; Published: 10 December 2019

Abstract: Heat exchanger designers need reliable thermal-hydraulic correlations to optimize heat exchanger designs. This work combines an adaptive sampling method with a Computational Fluid Dynamics (CFD) simulator to obtain increased accuracy and validity range of heat transfer and pressure drop predictions using a limited number of data points. Correlation efficacy was evaluated based on a steam generator case study. The sensitivity to the design parameters was analyzed in detail. The RMSE (root mean square error) of the developed correlations were reduced, through CFD sampling, from 28% to 15% for pressure drop, and from 33% to 25% heat transfer, compared to regression on experimental data only. The best reference correlations have RMSE values of 43% and 33% on pressure drop and heat transfer, respectively, on an independent validation set. Indeed, a radically different fin-tube geometry was suggested for the case study, compared to results using the Escoa correlations.The developed correlations show good to excellent agreement with trends in the CFD model. The quantitative error of predicted heat transfer and pressure drop coefficients at the case study optimum, however, was as large as those of the Escoa correlations. More data are likely needed to improve accuracy for compact heat exchanger designs further.

Keywords: numerical modeling; surrogate model; correlation; fin-tube; spiral fin-tube; CFD

1. Introduction

Increased energy efficiency is a key strategy to reduce anthropogenic CO_2 emissions, and often the most economical one in the industrial sector. Many energy intensive industries have already implemented measures such as heat integration and bottoming cycles up to its economic potential. An exception to this rule is the offshore oil and gas sector, where space and weight restrictions put severe limits to the amount of equipment that can be placed on each installation.

Volume and weight optimization of an offshore bottoming cycle is contingent on accurate thermal-hydraulic correlations. This is particularly true for the large and heavy waste heat recovery unit (WHRU), which typically consists of a circular fin-tube bundle. Numerical methods such as Computational Fluid Dynamics (CFD) can be used to predict the performance of such heat exchangers, but direct optimization is usually not feasible due to the large number of design variables and constraints and the computational cost (lead time) of each function evaluation.

Many thermal-hydraulic correlations for fin-tube bundles have been presented in the literature over the last half-century. Typically, correlations are algebraic expressions of non-dimensional groups with model constants fitted to experimental data by regression. The underlying data are derived from the authors' own published experimental work (e.g., [1]), from proprietary databases (e.g., [2]) or from a collection of several literature sources (e.g., [3]). In the two former cases, correlations tend to have a rather limited (or unknown) range of applicability. In the latter case, the underlying data are inherently scattered due to differences in experimental setups, data reduction methods and tube geometry details. This is particularly true for pressure drop measurements, where uncertainties are larger. Earlier work has shown that the WHRU skid weight can be reduced by scaling down the tube diameter to about 10 mm [4]. This requires new correlations with an extended validity range, to avoid extrapolation. There may also be a need to verify the accuracy of previously published work in a consistent manner.

Machine learning methods represent a contrasting approach to model building, where the model structure is less restricted. Artificial Neural Networks (ANN), Radial Basis function Neural Networks (RBNN) and Support Vector Regression (SVR) models have been used successfully to predict the thermal performance of a number of heat exchanger types. As shown in Table 1, most published studies utilize fully connected ANN models trained on experimental data. More recent publications have also considered other model setups, as well as sampling from a CFD model.

Table 1. Published work on thermal-hydraulic heat exchanger modeling using machine learning methods.

Data Source	Experimental	Correlation or CFD
Fully connected ANN	[5–10]	[11]
SVR, RBNN, Kriging	[9]	[12,13]

CFD models are increasingly being used for predictive design, even in critical applications such as nuclear reactor thermal-hydraulics [14], provided that rigorous verification and validation practices are adhered to. In the context of fin-tube bundles, CFD models can provide heat transfer and pressure drop coefficients in a consistent and time efficient manner. Comparisons with experimental data has shown good agreement, close to or within the experimental uncertainty, for a wide range of geometries [15]. CFD models are also able to provide data for extreme geometries that may not be possible to manufacture and test experimentally, but still add valuable data in the correlation development process. This includes "adversarial examples", i.e., geometries where small changes in parameters cause large changes in model output.

Given these developments, we propose to combine predictive CFD simulations with adaptive sampling and automated correlation building methodologies based on machine learning theory. We hypothesize that correlation accuracy and validity range can be increased simultaneously, with reasonable computational effort, by leveraging publicly available experimental work in conjunction with new, adaptively sampled simulation points. This paper provides the underlying simulated data points, in addition to the improved thermal-hydraulic correlations, to foster and accelerate further developments in the field. The presented methodology is applicable to a wide range of multivariate design problems where direct optimization with CFD is infeasible.

Specifically, the novelty of the investigation, as applied to fin-tube thermal-hydraulic correlation development, is the following:

- application of error estimation and adaptive sampling
- direct inclusion of predictive CFD model data in model regression
- extended validity range of geometric parameters towards the weight optimum indicated by earlier work

2. Method

The overall correlation building and verification process used in this article is shown in Figure 1. A design space relevant for waste heat recovery units was firstly defined (see Table 2). An initial database of experimental work from the

open literature was fed into the model building software ALAMO version 2018.4.3 [16].A correlation was generated and improved through adaptive sampling of data points from the CFD simulator. The correlation was then evaluated using a separate validation set, as well as a case study where the optimal point was compared to an independent CFD simulation. The validation set consists of 30 CFD simulations selected through Latin hypercube sampling of the design space, as indicated in Figure 1. Finally, the trends in the different input variables were evaluated using CFD simulations and compared to correlations from the present and earlier work. The remainder of this section describes the components of the methodology in further detail.

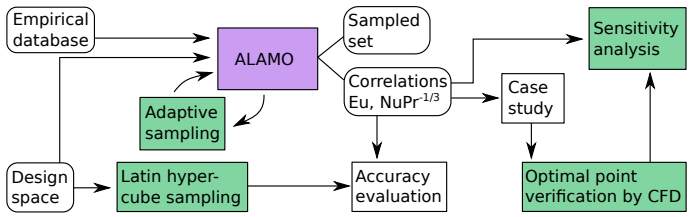

Figure 1. Process for correlation development, testing and benchmarking. Green boxes indicate where CFD simulations are employed.

Table 2. Considered design space for compact fin-tube bundles. Ancillary variables are adjusted to achieve a reasonable number of segments per fin revolution and a representative fin efficiency. Geometric parameters are shown in Figure 2.

Design Variables	**Min**	**Max**
$u_{F_{\min}}$ [m/s@500 °C]	2.53	30.4
d_o [mm]	9.65	50.8
h_f [mm]	1.4	25.4
h_s/h_f [-]	0.0	1.0
$\hat{s}_f$ [mm]	0.49	4.9
c_f [mm]	0.39	8.0
Ancillary and Derived Variables		
Re [-]	310	19,000
t_f [mm]	0.3	0.75
w_s [mm]	2.0	4.0
β [1] [deg]	30.0	30.0

[1] The tube bundle layout angle is defined as $\beta = \tan^{-1}\left(\frac{P_t}{2P_l}\right)$.

2.1. Initial Database

A database of published experimental work has previously been established at the Norwegian University of Science and Technology [17].The database contains data for 248 different fin-tube bundles from 21 publications, including both plain and serrated fin geometries. Several criteria were used to single out and prepare relevant data points for this study:

- Data points outside the ranges defined in Table 2 were omitted. The upper limit on $U_{F_{\min}}$ was relatively restrictive since kinematic viscosity for air is about three times higher at 500 °C compared to usual test conditions (∼100 °C). Hence, many experimental data points were excluded, but the resulting Reynolds number range (cf. Table 2). was considered representative of the possible operating conditions of a WHRU
- Geometries with only heat transfer or only pressure drop data were removed. A power law function was fitted to the heat transfer data of each remaining geometry and interpolated to the Reynolds numbers at which the (adiabatic) pressure drop was measured. This is necessary because the chosen model building method requires both outputs to be defined at each data point.
- A tube bank array of 30° was considered in this work, as it is the most compact arrangement. Tube banks with array angles in the range 25°–35° were corrected using Equation (1), derived from the Escoa correlation [18], to obtain data corresponding to $\beta = 30°$. The maximum applied corrections were 5% for the heat transfer data and 9% for the pressure drop data, respectively. Other tube bank data were discarded.
- The number of streamwise tube rows was not considered as a parameter in this work. Data point duplicates were removed such that only data for the largest number of tube rows were retained.

$$\begin{aligned} \mathrm{NuPr}_{30°} &= \mathrm{NuPr} \cdot \frac{1 + e^{-1/(2\tan\beta)}}{1 + e^{-1/(2\tan 30°)}}, \\ \mathrm{Eu}_{30°} &= \mathrm{Eu} \cdot \frac{1.1 + 1.8e^{-1/\tan\beta}}{1.1 + 1.8e^{-1/\tan 30°}} \end{aligned} \tag{1}$$

After this procedure, the remaining database contained 108 experimental data points.

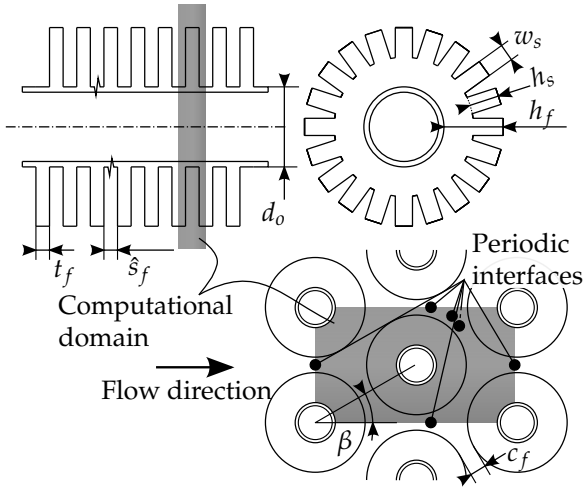

Figure 2. Geometric parameters of the fin-tube bundle and CFD computational domain.

2.2. Correlation Development (ALAMO)

ALAMO is a learning software that identifies simple, accurate surrogate models (correlations) using a minimal set of sample points from black box emulators such as experiments, simulations, and legacy code. ALAMO initially builds a low-complexity surrogate model using a best subset technique that leverages a mixed-integer programming formulation to consider a large number of potential functional forms. The model is subsequently tested, exploited, and improved through the use of derivative-free optimization solvers that adaptively sample new simulation or experimental points. For more information about ALAMO, see Cozad et al. [16,19] and Wilson and Sahinidis [20].

The functional form of a regression model was assumed to be unknown to ALAMO. Instead, several simple basis functions were proposed, e.g., x, x^2, $1/x$, $\log(x)$, and a constant. Once a set of potential basis functions was collected, ALAMO attempted to construct the lowest complexity function that accurately models the initial training data. This model was obtained by minimizing the Bayesian information criterion, $BIC = SSR_p/\hat{\sigma} + p\log(n)$, where p is the number of included basis functions, SSR_p is the sum of squared residuals for the selected model, and $\hat{\sigma}$ is an estimation for the variance of the residuals, which is obtained using the least squares solution of the full basis set or can be specified a priori. The model fitness metric (BIC) was rigorously minimized using a combination of enumeration, heuristics, and eventual global optimization using the BARON solver [21].

Combinations of linear terms and fractions of the input variables were considered for this particular application, as well as selected powers of these functions with an exponent smaller than unity. Binomial terms, and powers of these, were also considered in modeling the Nusselt number. Once a model was identified, it was improved systematically in ALAMO using an adaptive sampling technique that added new simulation or experimental points to the training set. New sample points were selected to maximize model inconsistency in the original design space, as defined by box constraints on x, using derivative-free optimization methods [22]. It was observed that a higher correlation accuracy was obtained if the outputs and the velocity-related input were log-transformed. It is well known that the velocity dependence is essentially logarithmic and therefore easier to model in log space. As an additional benefit, correlation terms become multiplicative rather than additive. This facilitates interpretation of the correlation as consisting of one velocity-dependent term multiplied with a number of "geometry correction" terms.

2.3. Numerical Model

Numerical simulations in this work followed the methodology described in a previous article [15], where thorough validation with experimental data are given. The main characteristics of the numerical model are as follows:

- Fully periodic computational domain (Figure 2) was discretized primarily with hexahedral cells. A graded boundary layer grid was used in the wall normal direction in the space between the fins ($y^+ < 1$).
- Density and thermophysical properties were considered constant, properties for air were used for the external fluid and the fin thermal conductivity was set corresponding to carbon steel ($48.5\,\mathrm{W\,m^{-1}\,K^{-1}}$).
- The steady-state Reynolds Averaged Navier–Stokes (RANS) equations were solved together with the energy equation and the Spalart–Allmaras turbulence model equation [23] using the open source CFD toolbox OpenFOAM v4.1.
- The Spalart–Allmaras turbulence model was selected due to its simplicity, robustness and suitability for simulating boundary layers under adverse pressure gradient conditions. It also yields similar results as other eddy viscosity turbulence models when applied to finned tube bundles [24]. Model constants were kept at their default value, including the turbulent Prandtl number.
- Second order upwind discretization was used for all convective terms.
- The conjugate heat transfer between the fin and the external fluid was modeled explicitly, resolving the temperature field in the fin. The tube

wall thermal resistance was neglected—a uniform temperature was applied at the fin root and on the tube surface. The fluid bulk temperature was specified at the leftmost periodic boundary, avoiding source terms in the energy equation.

- Fin efficiency was evaluated by solving the energy equation a second time, subsequent to RANS model convergence, assuming a frozen flow field and a uniform temperature boundary condition on one fin-tube row. The resulting heat flux was used to compute the fin efficiency in the first simulation having finite thermal conductivity in the fin.
- The computed heat flux, bulk temperature and total pressure drop were normalized into Nusselt and Euler numbers according to standard practice (see, e.g., [17]).

2.4. Accuracy Evaluation

The accuracies of the correlations were evaluated based on the coefficient of determination (R^2) and root mean square error (RMSE) values on an independent dataset sampled using CFD ($N = 30$). Some samples struggled to reach iterative convergence during CFD simulation, in which case the flow velocity was reduced. The RMSE is expressed in terms of the deviation from the observed values, viz.

$$\mathrm{RMSE} = \sqrt{\frac{1}{N}\sum_{N}\left(\frac{y_i - f_i}{y_i}\right)^2} \tag{2}$$

for the predicted values f_i (from correlations) and the observed values y_i (from CFD simulations). Note that the RMSE is equal to the standard deviation for an unbiased estimator.

2.5. Case Study and Verification of Optimal Point

A case study was defined to test the developed correlation on a realistic optimization task and compare the computed optimal point to that obtained using a reference correlation. The predicted heat transfer and pressure drop coefficients were also compared to those predicted by CFD simulations. A boiler section of a generic offshore heat recovery steam generator was considered, with the steam and exhaust gas specifications and constraints given in Table 3. The tube wall temperature was considered constant, and heat conduction through the tube wall, as well as steam/water pressure drop, was neglected. This leads to a computationally cheap heat balance, which can be evaluated using the ϵ-NTU method as a function of the exhaust mass flow, cold end temperature

difference, and gas side heat transfer coefficient. The objective function is the fin-tube bundle weight, where the tube wall thickness is calculated as

$$t_w = 1.1 \frac{p_s(d_o/2)}{0.85\sigma_y + 0.4p_s} \tag{3}$$

where p_s is the steam pressure and σ_y is the yield stress of carbon steel at 500 °C. The fins were assumed to be made from carbon steel ($\lambda = 48.5\,\mathrm{W\,m^{-1}\,K^{-1}}$, $\rho = 7850\,\mathrm{kg\,m^{-3}}$). A theoretical fin efficiency according to Hashizume et al. [25] was used. The ideal gas law was used to evaluate the exhaust gas density at the average bulk temperature, and all other physical properties were considered constant.

Table 3. Boiler section case study: Definitions and constraints.

Exhaust mass flow [kg/s]	75.0
Exhaust pressure drop [Pa]	1500
Steam pressure [Pa]	25×10^5
Steam/water temperature [°C]	224
Cold end temperature difference [°C]	20
Transferred heat [W]	$\geq 15 \times 10^6$
Narrow gap flow velocity [m/s]	≤ 30
Frontal cross-section	square

The number of tube rows in the transverse and longitudinal directions were modeled as real numbers to obtain a smooth objective function. N_r was calculated directly from the pressure drop constraint, whereas N_t was a free variable. Remaining free variables and bounds were equal to the design variables and bounds in Table 2, with the fin thickness lower bound set to 0.5 mm and w_s adjusted to give 20 segments per revolution for serrated fins. A tube bundle layout angle of 30° was used throughout.

The optimization problem was solved in MATLAB R2017a using the built-in function *fmincon* that implements the SQP algorithm. The optimization was repeated 100 times for a given case, using random starting points within the design space, to ensure that a global, feasible optimum point was reached.

3. Results and Discussion

3.1. Correlation Development

The accuracy evaluation (Table 4) confirmed a relatively good fit between the developed correlations and the independently sampled validation set. The coefficient of determination is high for the Euler number, but less impressive for the Nusselt number. The RMSE is acceptable for the Euler number, but quite

large for the Nusselt number, particularly when considering that the 95% confidence interval is much wider than the RMSE.

Table 4. Accuracy on validation dataset, computed from Latin hypercube sample of design space (30 CFD simulations).

Model	Eu		$NuPr^{-1/3}$	
	R^2 [-]	RMSE [%]	R^2 [-]	RMSE [%]
This work				
database only	0.75	28	0.70	33
after sampling	0.94	15	0.76	25
Holfeld [17]	−0.08	58	0.75	35
Escoa [18]	−0.05	43	0.42	34
PFR [26]	0.79	72	0.59	33

The difficulty in modeling the Nusselt number may be due to complex changes in the flow field, whereby the flow bypasses the aperture between the fins and flow outside the fin diameter for certain geometric configurations (typically low fin apertures and large fin tip clearances). This phenomenon has been more thoroughly discussed in [27], but ultimately necessitates a different modeling approach than the current one due to the large nonlinearity involved.

The predictive accuracies for the reference correlations (Holfeld [17], Escoa [18] and PFR [26]) are, in general, poor due to the severe extrapolation induced by the design space definition. As shown in Figure 3, the general scatter for the reference correlations on all data in this work (empirical database, adaptively sampled simulations and simulations used for validation) is large, particularly for low Reynolds numbers. The PFR correlation for Eu has a relatively high coefficient of determination compared to the Escoa and Holfeld correlations, indicating that the hydraulic diameter (which is the unique feature of the PFR Eu correlation) may be a more robust length scale than the tube diameter. The high RMSE associated with the PFR Eu correlation is due to a positive bias (overprediction) that would be simple to rectify with a constant correction factor.

The detailed functional form of the developed correlations is further discussed in Section 3.3. Algebraic expressions of the correlations are provided in the Appendix A.

3.2. Case Study

Results from the case study consist of four optimized geometries, two for each correlation with and without an explicit tube diameter constraint,

respectively. Geometries and thermal-hydraulic results are given in Table 5 and 3D representations of the two geometries without diameter constraints are shown in Figure 4.

Clearly, two different strategies towards fulfilling the heat duty under a pressure drop constraint emerge for the two different correlations. The optimal geometry for the correlations developed in this work is extremely compact (dense) with a few number of tube rows and a high surface area per tube, but a large frontal area. The optimal geometry using the Escoa correlations, on the other hand, aim to reduce the Euler number such that a larger number of tube rows can be afforded under the pressure drop constraint. This results in a smaller frontal area and a more "open" geometry with less heat transfer area per tube.

Note that the tube diameter reaches its lower bound, and the flow velocity its upper bound, for both correlations. This result is as expected, since the Nusselt number ($=\alpha_o d_o/\lambda_{\text{air}}$) scales with approximately $\text{Re}^{0.7}$ and therefore $\alpha_o \propto \text{Re}^{0.7}/d_o \propto d_o^{-0.3}$ for a constant velocity. The heat transfer area scales with the perimeter of the tube (disregarding the fins for a moment), leading to $\alpha_o A_t \propto d_o^{0.7}$. The Euler number (i.e., the pressure drop), on the other hand, scales with $d_o^{-0.3}$ at best. This mean that the heat transfer coefficient decreases at the same rate as the pressure drop. A hypothetical doubling of the tube diameter changes the transferred heat by a factor of $2^{0.7} = 1.62$ and the pressure drop by a factor of $2^{-0.3} = 0.812$. If the number of tube rows are increased accordingly (to utilize the available pressure drop), the transferred heat can be increased to $1.62/0.812 = 2.0$ and the transferred heat per unit surface area is the same as for the smaller tubes. The *weight* of the larger tubes, however, is higher than the smaller tubes due to a larger wall thickness and larger internal fluid volume. The only caveat to the argument for a small tube diameter is that restrictions on the steam side pressure drop, steam side heat transfer coefficient, boiling stability and heat exchanger frontal area are not considered here. Moreover, large diameter tubes are less susceptible to flow induced vibrations due to a higher bending stiffness.

Optimization with a fix tube diameter show that similar geometries are obtained as when the tube diameter is free, only with larger frontal area, fewer tube rows and a higher total weight.

Table 5. Case study: Geometry optima for correlations from this work and Escoa, without (left column) and with explicit diameter constraint of 25.4 mm (right column). Eu and $\mathrm{NuPr}^{-1/3}$ data are computed at the closest geometry possible to simulate with CFD

Correlations: Geometry	**This Work**		**Escoa**	
Re [-]	3600	9400	3600	9400
d_o [mm]	9.65	25.4	9.65	25.4
h_f [mm]	10.9	12.7	6.28	15.8
h_s/h_f [mm]	1.0	1.0	0.96	1.0
t_f [mm]	0.50	0.50	0.50	0.50
$\hat{s}_f$ [mm]	0.49	0.49	4.90	4.90
w_s [mm]				
c_f [mm]	0.39	0.39	8.00	8.00
N_r [-]	2.2	1.2	21.8	17.1
N_t [-]	140	102	105	52
Normalized objective function	1.00	1.49	0.87	2.33
Eu [-]				
This work	5.64	10.8		
Escoa			0.594	0.76
CFD	3.81	6.28	0.52	0.75
Deviation [%]	+48	+72	+13	−2.2
$\mathrm{NuPr}^{-1/3}$ [-]				
This work	66.6	125.0		
Escoa			56.8	96.5
CFD	67.7	136	38.9	74.4
Deviation [%]	−1.7	−8.0	−46	+30

The correlation accuracy at the optima, quantified by the deviations from the CFD simulation results, showed mixed performance. The pressure drop was grossly overpredicted by the correlation developed in this work, whereas the heat transfer coefficient was grossly overpredicted by the Escoa correlation. The normalized objective function should therefore be interpreted with care. The optimized geometry using correlations from this work turn out to be conservative (would satisfy heat duty and pressure drop constraints), whereas the optimized Escoa geometries would transfer too little heat.

However, the *trends* in the prediction of the design variables may be just as important as the accuracy at the optimum, since these trends determine the *location* of the optimum to begin with. This is the topic of the sensitivity analysis.

3.3. Sensitivity Analysis

The trends in Eu and Nu with respect to the flow velocity and the five geometric variables are shown, for perturbations around the midpoint of the design space, in Figures 5 and 6. These figures also include independent CFD simulations (not included in the training data) at the optimum and at perturbations around the optimum (with remaining variables held constant). Corresponding figures for perturbations around the optimal point in the case study are Figures 7 and 8.

The Euler number exhibits a high sensitivity to the flow velocity and the fin aperture compared to the other four variables (Figures 5 and 7). The velocity dependence can be explained as a transition from friction dominated drag to a mix of friction and form drag as velocity increases. At the design space midpoint, both of these pressure losses seem to be of equal importance, since the sensitivity to increases in wake size (d_o) and increases in friction area (h_f) is about the same. At the optimum point, a higher sensitivity to the wake size relative to friction area can be noticed (Figure 7, top middle and top right panels) due to the higher flow velocity.

The sensitivity to the fin aperture at constant mean flow velocity should be interpreted in light of the small fin pitches used in this work. Not only does a smaller fin aperture mean more friction area per unit tube length, but also corresponds to a higher maximum flow velocity between the fins required to maintain the same mean velocity. In other words, the blockage caused by the boundary layers on the fins is significant compared to the available cross-sectional (flow) area for the considered range of fin apertures. The lack of a positive correlation between the Euler number and the degree of serration (h_s/h_f) is unexpected, given that serrations break up the fin boundary layer and hence decrease the average boundary layer thickness. On the other hand, the correlation between h_s/h_f and the Nusselt number is also small and, therefore, consistent with the Euler number results. These observations point towards a conclusion that the thermal-hydraulic benefit of serrated fins lie primarily in the increased fin efficiency.

The Nusselt number is primarily a function of the flow velocity and the tube diameter (Figures 6 and 8). Considering that $\mathrm{Nu} = \alpha_o d_o/\lambda_{\mathrm{air}}$, i.e., linear in d_o, the heat transfer coefficient is approximately constant with the tube diameter as well as with the other geometric parameters. This can be expected in this case, since the heat transfer resistance consists of external boundary layers.

A trend change in $\hat{s}_f$ can be noted when comparing sensitivities at the midpoint and the optimal point (lower middle panels, Figures 6 and 8): The Nusselt number is relatively constant at the midpoint, but shows a clear negative trend at the optimal point. A possible explanation involves the already

mentioned bypass effect. At the midpoint, a decrease in $\hat{s}_f$ increases the pressure drop (Figure 5), but also redistributes the flow to the passage outside the fin perimeter. The increased pressure drop does not translate to an increased heat transfer coefficient (Figure 6). A small fin tip gap on the other hand, such as at the optimal point, suppresses the bypass effect and forces the flow to pass through the fin aperture. Hence, a decrease in $\hat{s}_f$ does translate into both increased pressure drop and heat transfer coefficient. The effect is further discussed in [27].

The reference correlations exhibit the correct variable *trend* in most cases. The PFR correlations captures the trend around the optimal point to a surprising degree, given its simplicity. The quantitative accuracy of the reference correlations, however, is not satisfactory at the optimal point. The Holfeld correlations, which are the most recently developed, grossly underpredict the pressure drop and show incorrect trends for Eu as a function of d_o and Nu as a function of $\hat{s}_f$.

The correlations developed in this work generally agree well with the CFD simulations. Trends in h_f and c_f are exaggerated at the case study optimum, most likely due to limited amount of data in the design space, but generally provides improved prediction accuracy.

4. Conclusions

Machine learning methods, including adaptive sampling using a CFD simulator, has been used to improve the accuracy and validity range of thermal-hydraulic correlations for fin-tube bundles, in terms of both the coefficient of determination (R^2) and the root mean square error. The applicability to geometry optimization was verified through a case study and the accuracy of the modeling of trends in the design space was confirmed by comparison with CFD simulations. The following specific conclusions can be drawn:

- The choice of correlation is decisive for the outcome of tube bundle weight optimization, at least for the boiler section considered in the case study. The developed correlations suggest a radically different design compared to the Escoa correlations.
- The trends of the developed correlations generally match well with data from the CFD model. The sensitivity to the design variables close to the optimal point for the case study is, however, exaggerated for some variables.
- The PFR correlation for the Euler number is the most robust reference correlation with regards to the trends in the design variables, indicating that the hydraulic diameter can be an appropriate length scale for pressure drop modeling.

- The Nusselt number is relatively insensitive to all design parameters other than the flow velocity and the tube diameter (i.e., the Reynolds number) around the studied design points.
- In general, the Nusselt number appears more difficult to model accurately, compared to the Euler number. A possible explanation, given the preceding bullet point, is that particular geometries cause complex flow redistribution that only a highly nonlinear model can represent.
- Quantitative accuracy on the case study is good for the developed heat transfer correlation, but disappointing for the pressure drop correlation. The accuracy of the Escoa correlations is also poor at the case study optimum. More data are most likely needed in the range of compact designs with low tube diameter, if further accuracy improvements are to be achieved.

The machine learning approach appears to be a viable method to extend the validity range of thermal-hydraulic correlations, with relatively moderate resource usage. As ever, the dataset size limits the model nonlinearity that can be used without overfitting to the training data. Further increase in accuracy will, most likely, require significantly larger datasets created by a combination of structured sampling methods (e.g., Latin hypercube) and adaptive sampling methods.

A limitation of the current study is that the correlation accuracy is restricted to the accuracy of the numerical model. The numerical model is successfully validated over a large range of geometric parameters for which experimental data exist [15]; Future directions of this work should therefore include experimental investigations of previously untested geometries indicated by the correlations, such as at the case study optimum indicated in this work.

Supplementary Materials: The following are available online at http://www.mdpi.com/1996-1073/xx/1/0/s1, Table S1: Underlying CFD simulation data: regression data points, Table S2: Underlying CFD simulation data: validation data points.

Author Contributions: Conceptualization, K.L., E.N. and N.V.S.; Methodology, Z.W., N.V.S. and K.L.; Software, Z.W. and N.V.S.; Formal analysis, K.L. and Z.W.; Investigation, K.L. and Z.W.; Data curation, K.L. and E.N.; Writing—original draft preparation, K.L. and Z.W.; Writing—review and editing, N.V.S. and E.N.; Visualization, K.L.; and Supervision, N.V.S. and E.N.

Funding: K.L. and E.N. acknowledge the partners: Neptune Energy Norge AS, Alfa Laval, Equinor, Marine Aluminium, NTNU, SINTEF and the Research Council of Norway, strategic Norwegian research program PETROMAKS2 (#233947) for their support KL further acknowledges the travel support from Hans Mustad og Robert og Ella Wenzins legat ved Norges teknisk- naturvitenskapelige universitet that enabled the visit at Carnegie Mellon University.

Conflicts of Interest: The authors declare no conflict of interest. The funding sponsors has approved the decision to publish the results, but had no role in the design of the study; in the collection, analyses, or interpretation of data or in the writing of the manuscript.

Abbreviations

The following abbreviations are used in this manuscript:

ALAMO	Automated Learning of Algebraic Models for Optimization
ANN	Artificial Neural Network
BIC	Bayesian Information Criterion
CFD	Computational Fluid Dynamics
RANS	Reynolds Average Navier–Stokes
RBNN	Radial Basis function Neural Network
RMSE	Root Mean Square Error
SVR	Support Vector Regression
WHRU	Waste Heat Recovery Unit

Nomenclature

Roman symbols	
A_f	fin heat transfer area [m^2]
A_t	tube heat transfer area [m^2]
c_f	fin tip-to-tip clearance [m]
d_o	outer tube diameter [m]
h_f	total fin height [m]
h_s	segmented height [m]
N_r	number of streamwise tube rows [-]
N_t	number of transverse tube rows [-]
p	total pressure [Pa]
P_t	transverse tube pitch [m]
P_l	longitudinal tube pitch [m]
s_f	fin pitch [m]
$\hat{s}_f$	fin aperture (=$s_f - t_f$) [m]
t_f	fin thickness [m]
t_w	tube wall thickness [m]
$u_{F_{min}}$	mean velocity in minimum free flow area [$m\,s^{-1}$]
w_s	segment width [m]
Greek symbols	
α_o	outer heat transfer coefficient [$W\,m^{-2}\,K^{-1}$]
β	tube bundle layout angle [°]
η_f	fin efficiency [-]
λ	thermal conductivity [$W\,m^{-1}\,K^{-1}$]
ν	kinematic viscosity [$m^2\,s^{-1}$]
$\tilde{\nu}$	modified turbulent viscosity [$m^2\,s^{-1}$]
ρ	density [$kg\,m^{-3}$]
σ_y	yield stress [-]
Dimensionless numbers	
$\mathrm{Re} = u_{F_{\mathrm{min}}} d_o / \nu$	Reynolds number
$\mathrm{Eu} = \Delta p / \left(N_r \frac{1}{2} \rho u_{F_{\mathrm{min}}}^2 \right)$	Euler number
$\mathrm{Nu} = \alpha_o d_o / \lambda$	Nusselt number
$\mathrm{Pr} = \nu \rho c_p / \lambda$	Prandtl number

Appendix A

Algebraic expressions for the regression models developed in this work are given in Equations (A1) and (A2). All dimensions (d_o, h_f, etc.) *must* be in millimeters due to the dimensional nature of some of the regression constants.

$$\begin{aligned}\mathrm{Eu} = \left(\frac{\mathrm{Re}}{d_o}\right)^{-0.420} & 0.990^{d_o} 0.971^{h_f} 1.04^{c_f} \\ & \cdot 0.00246^{\left(\frac{\log_{10}(\mathrm{Re}/d_o)}{d_o}\right)^{0.2}} 137^{\left(\frac{\log_{10}(\mathrm{Re}/d_o)}{h_f}\right)^{0.2}} 12.5^{\left(\frac{h_f}{\hat{s}_f}\right)^{0.2}} \\ & \cdot 0.778^{\left(\frac{d_o}{h_f}\right)^{0.6}} 1.27^{\left(\frac{h_f}{\hat{s}_f}\right)^{0.6}} 0.685^{\left(\frac{c_f}{\hat{s}_f}\right)^{0.6}} \end{aligned} \quad \text{(A1)}$$

$$\begin{aligned}\mathrm{NuPr}^{-1/3} = \mathrm{Re}^{0.637} & 0.996^{h_f} 0.511^{(c_f/\hat{s}_f)^{0.5}} \\ & \cdot 1.26^{\left(\log_{10}(\mathrm{Re}/d_o) * \frac{h_s}{h_f}\right)^{0.2}} 0.262^{\left(\log_{10}(\mathrm{Re}/d_o) * \hat{s}_f\right)^{0.2}} \\ & \cdot 2.14^{\left(\log_{10}(\mathrm{Re}/d_o) * c_f\right)^{0.2}} \end{aligned} \quad \text{(A2)}$$

References

1. Ma, Y.; Yuan, Y.; Liu, Y.; Hu, X.; Huang, Y. Experimental investigation of heat transfer and pressure drop in serrated finned tube banks with staggered layouts. *Appl. Therm. Eng.* **2012**, *37*, 314–323. doi:10.1016/j.applthermaleng.2011.11.037.
2. Weierman, C. Correlations ease the selection of finned tubes. *Oil Gas J.* **1976**, *74*, 10–94.
3. Nir, A. Heat transfer and friction factor correlations for crossflow over staggered finned tube banks. *Heat Transf. Eng.* **1991**, *12*, 43–58. doi:10.1080/01457639108939746.
4. Skaugen, G.; Walnum, H.T.; Hagen, B.A.L.; Clos, D.P.; Mazzetti, M.; Nekså, P. Design and optimization of waste heat recovery unit using carbon dioxide as cooling fluid. In Proceedings of the ASME 2014 Power Conference, Baltimore, MD, USA, 28–31 July 2014; pp. 1–10.
5. Pacheco-Vega, A.; Sen, M.; Yang, K.T.; McClain, R.L. Neural network analysis of fin-tube refrigerating heat exchanger with limited experimental data. *Int. J. Heat Mass Transf.* **2001**, *44*, 763–770. doi:10.1016/S0017-9310(00)00139-3.
6. Islamoglu, Y. A new approach for the prediction of the heat transfer rate of the wire-on-tube type heat exchanger - Use of an artificial neural network model. *Appl. Therm. Eng.* **2003**, *23*, 243–249. doi:10.1016/S1359-4311(02)00155-2.

7. Islamoglu, Y.; Kurt, A. Heat transfer analysis using ANNs with experimental data for air flowing in corrugated channels. *Int. J. Heat Mass Transf.* **2004**, *47*, 1361–1365. doi:10.1016/j.ijheatmasstransfer.2003.07.031.
8. Xie, G.N.; Wang, Q.W.; Zeng, M.; Luo, L.Q. Heat transfer analysis for shell-and-tube heat exchangers with experimental data by artificial neural networks approach. *Appl. Therm. Eng.* **2007**, *27*, 1096–1104. doi:10.1016/j.applthermaleng.2006.07.036.
9. Peng, H.; Ling, X. Predicting thermal-hydraulic performances in compact heat exchangers by support vector regression. *Int. J. Heat Mass Transf.* **2015**, *84*, 203–213. doi:10.1016/j.ijheatmasstransfer.2015.01.017.
10. Hassan, M.; Javad, S.; Amir, Z. Evaluating different types of artificial neural network structures for performance prediction of compact heat exchanger. *Neural Comput. Appl.* **2017**, *28*, 3953–3965. doi:10.1007/s00521-016-2302-z.
11. Thibault, J.; Grandjean, B.P.A. A neural network methodology for heat transfer data analysis. *Int. J. Heat Mass Transf.* **1991**, *34*, 2063–2070. doi:10.1016/0017-9310(91)90217-3.
12. Koo, G.W.; Lee, S.M.; Kim, K.Y. Shape optimization of inlet part of a printed circuit heat exchanger using surrogate modeling. *Appl. Therm. Eng.* **2014**, *72*, 90–96. doi:10.1016/j.applthermaleng.2013.12.009.
13. Shi, H.N.; Ma, T.; Chu, W.X.; Wang, Q.W. Optimization of inlet part of a microchannel ceramic heat exchanger using surrogate model coupled with genetic algorithm. *Energy Convers. Manag.* **2017**, *149*, 988–996. doi:10.1016/j.enconman.2017.04.035.
14. Bauer, R.C. A framework for implementing predictive-CFD capability in a design-by-simulation environment. *Nuclear Technol.* **2017**, *200*, 177–188. doi:10.1080/00295450.2017.1360715.
15. Lindqvist, K.; Næss, E. A validated CFD model of plain and serrated fin-tube bundles. *Appl. Therm. Eng.* **2018**, *143*, 72–79. doi:10.1016/j.applthermaleng.2018.07.060.
16. Cozad, A.; Sahinidis, N.V.; Miller, D.C. Learning surrogate models for simulation-based optimization. *AIChE J.* **2014**, *60*, 2211–2227. doi:10.1002/aic.14418.
17. Holfeld, A. Experimental Investigation of Heat Transfer and Pressure Drop in Compact Waste Heat Recovery Units. Ph.D. Thesis, Norwegian University of Science and Technology, Trondheim, Norway, 2016.
18. ESCOA Fintube Corp. ESCOA Engineering Manual (Electronic Version). Technical Report. 2002. Available online: http://www.fintubetech.com/escoa/ (accessed on 1 September 2005).
19. Cozad, A.; Sahinidis, N.V.; Miller, D.C. A combined first-principles and data-driven approach to model building. *Comput. Chem. Eng.* **2015**, *73*, 116–127. doi:10.1016/j.compchemeng.2014.11.010.
20. Wilson, Z.T.; Sahinidis, N.V. The ALAMO approach to machine learning. *Comput. Chem. Eng.* **2017**, *106*, 785–795. doi:10.1016/j.compchemeng.2017.02.010.

21. Kılınç, M.; Sahinidis, N.V. Exploiting integrality in the global optimization of mixed-integer nonlinear programming problems in BARON. *Optim. Methods Soft.* **2019**, *33*, 540–562.
22. Rios, L.M.; Sahinidis, N.V. Derivative-free optimization: A review of algorithms and comparison of software implementations. *J. Glob. Optim.* **2013**, *56*, 1247–1293. doi:10.1007/s10898-012-9951-y.
23. Spalart, P.; Allmaras, S. A one-equation turbulence model for aerodynamic flows. *La Reserche Aérospatiale* **1994**, *1*, 5–21.
24. Nemati, H.; Moghimi, M. Numerical Study of Flow Over Annular-Finned Tube Heat Exchangers by Different Turbulent Models. *CFD Lett.* **2014**, *6*, 101–112.
25. Hashizume, K.; Morikawa, R.; Koyama, T.; Matsue, T. Fin Efficiency of Serrated Fins. *Heat Transf. Eng.* **2002**, *23*, 6–14. doi:10.1080/01457630252800386.
26. PFR Engineering Systems Inc. *Heat Transfer and Pressure Drop Characteristics of Dry Tower Extended Surfaces*; Technical Report, PFR Report BNWL-PFR-7-100; PFR Engineering Systems Inc.: Sante Fe Springs, CA, USA, 1976.
27. Lindqvist, K.; Næss, E. On correction factors in thermal-hydraulic correlations for compact fin-tube bundles. *Heat Mass Transf.* **2018**, submitted.

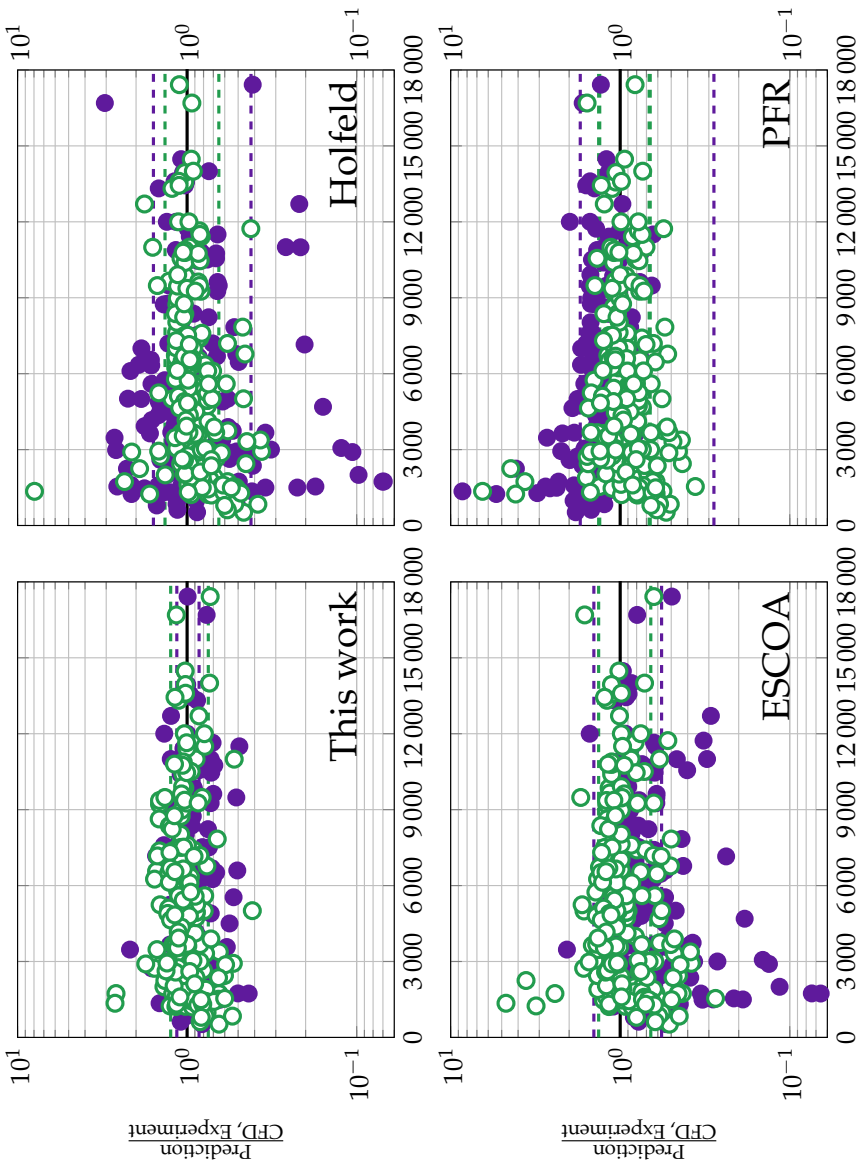

Figure 3. Predictive accuracy on regression and validation data (208 data points): correlations developed in this work and correlations from Holfeld [17], Escoa [18] and PFR [26].

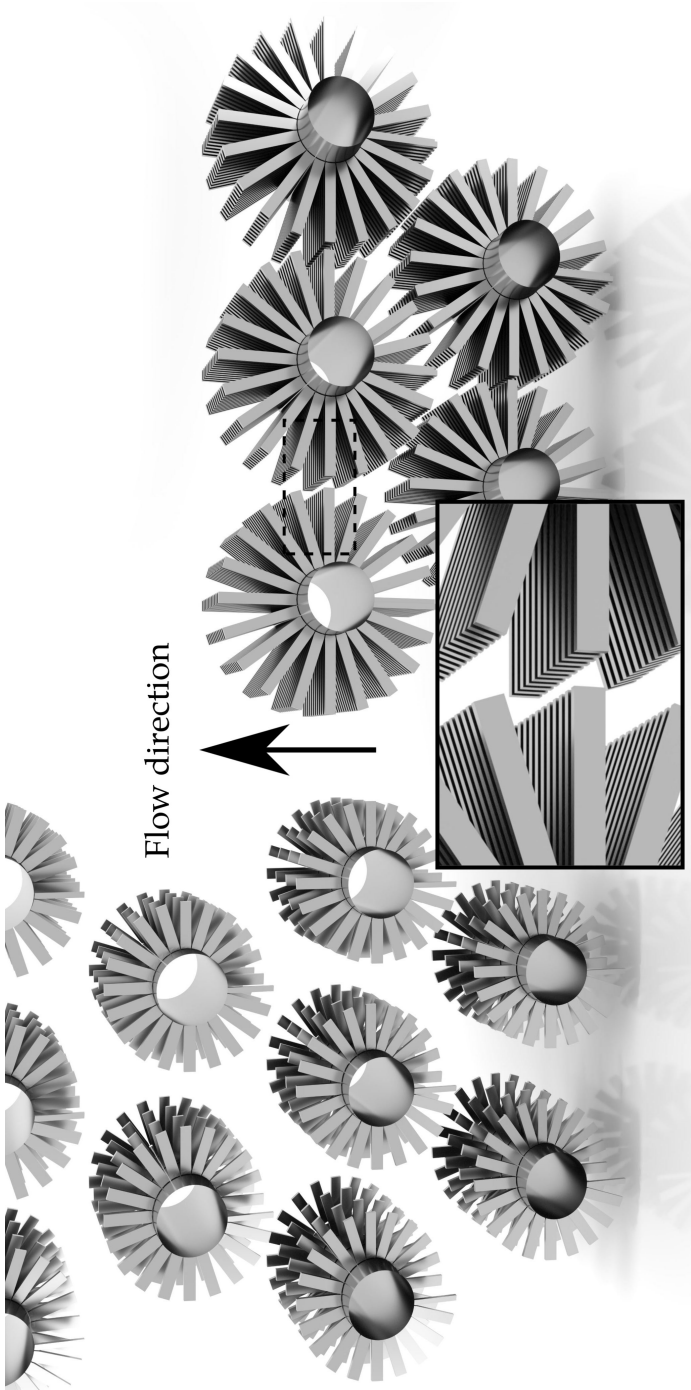

Figure 4. Optimized boiler geometry using the Escoa correlations (**left**) and correlations developed in this work (**right**), without explicit diameter constraints

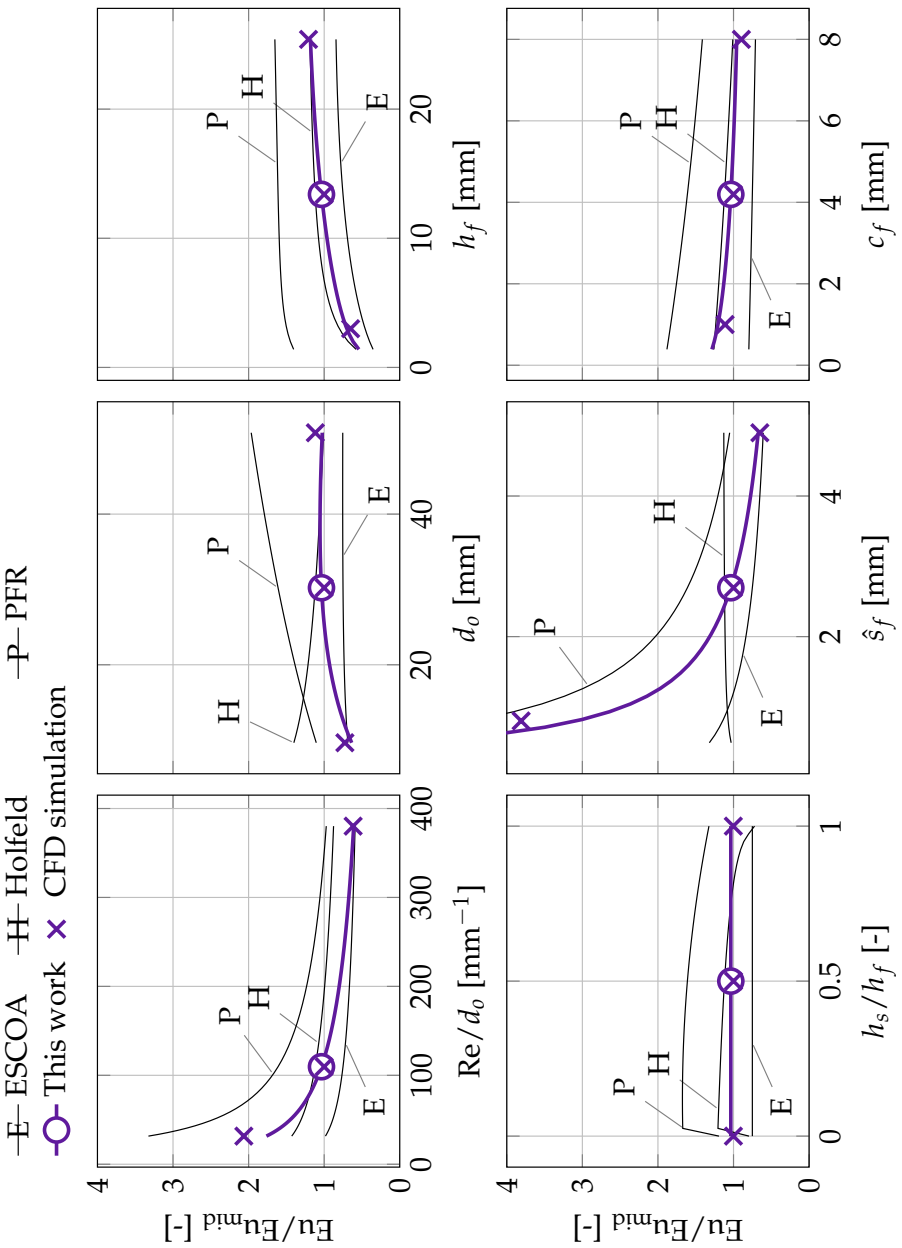

Figure 5. Trends in correlations and CFD simulator around the midpoint in the design space (marked by a circle). CFD simulations were independently sampled (not part of the dataset used for model development). Each parameter was varied independently, with remaining parameters held constant.

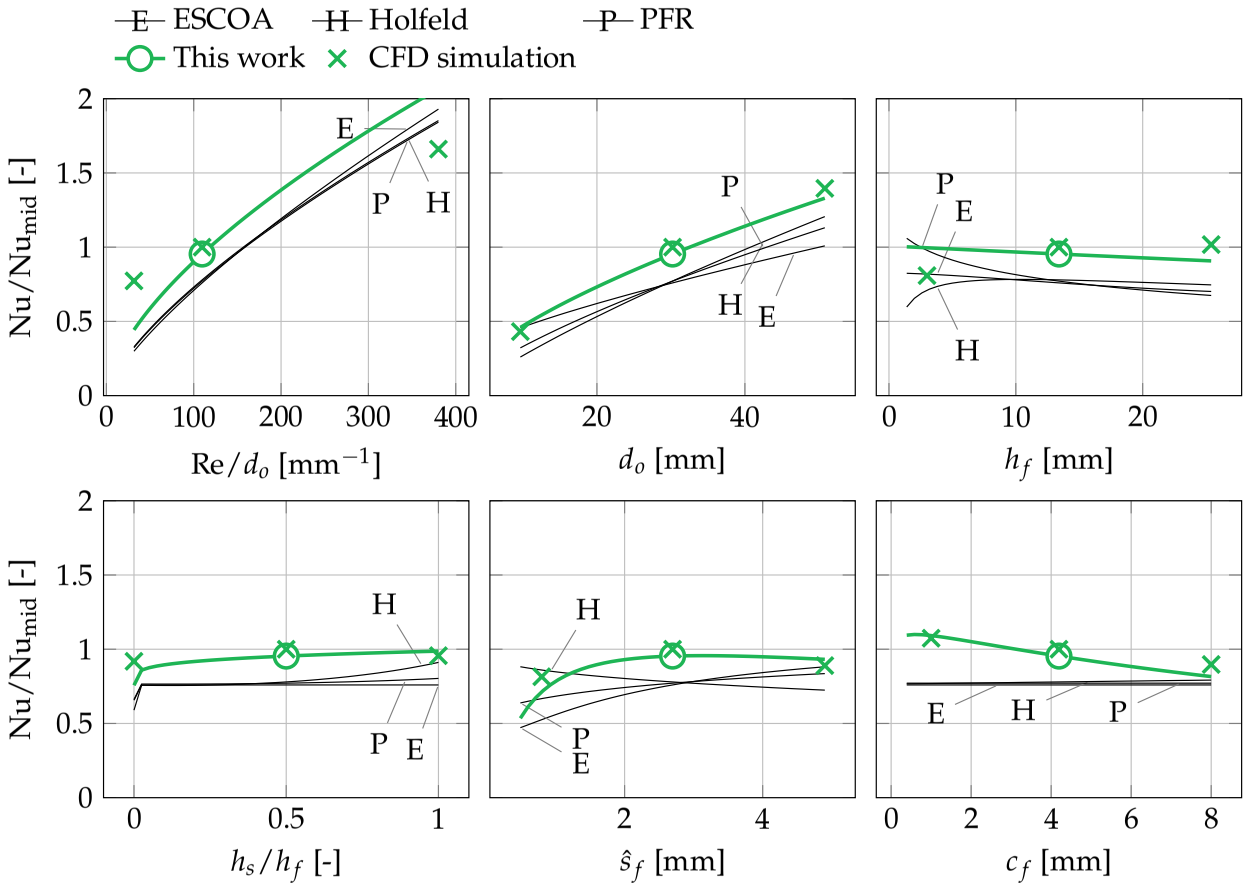

Figure 6. Trends in correlations and CFD simulator around the midpoint in the design space (marked by a circle). CFD simulations were independently sampled (not part of the dataset used for model development). Each parameter was varied independently, with remaining parameters held constant.

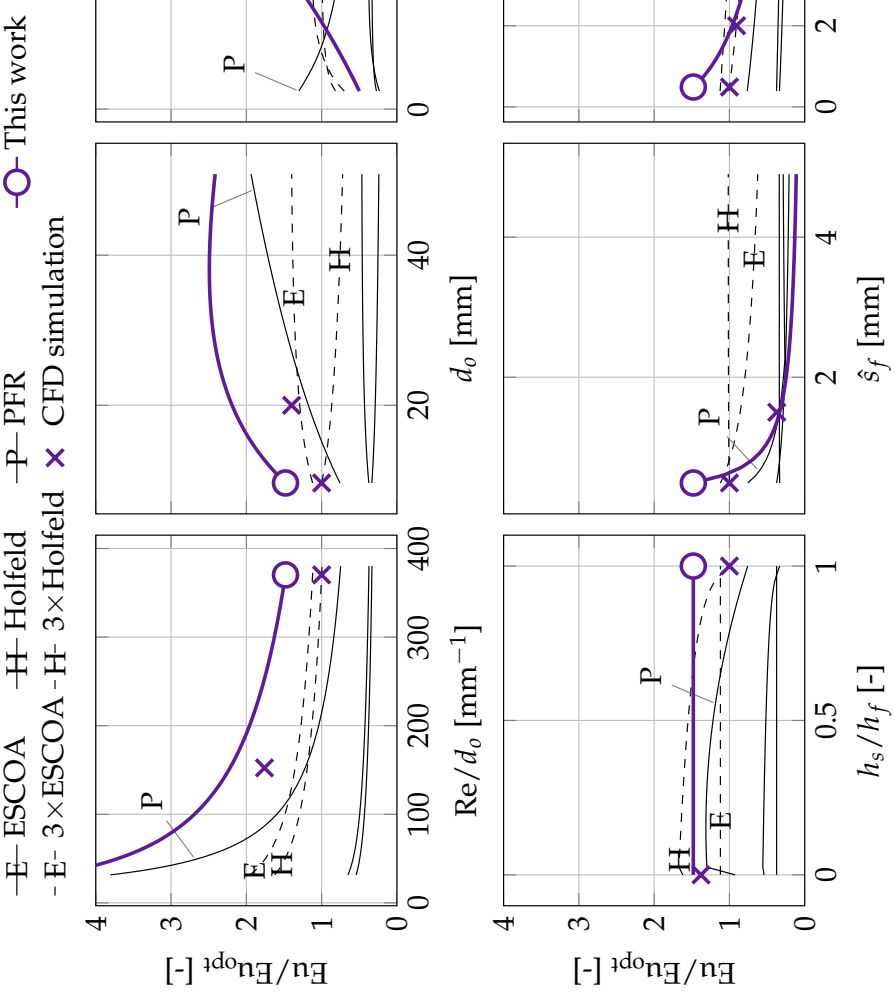

Figure 7. Trends in correlations around the case study optimum found using correlations developed in this work (marked by a circle). CFD simulations were independently sampled (not part of the dataset used for model development). Each parameter was varied independently, with remaining parameters held constant at the optimum.

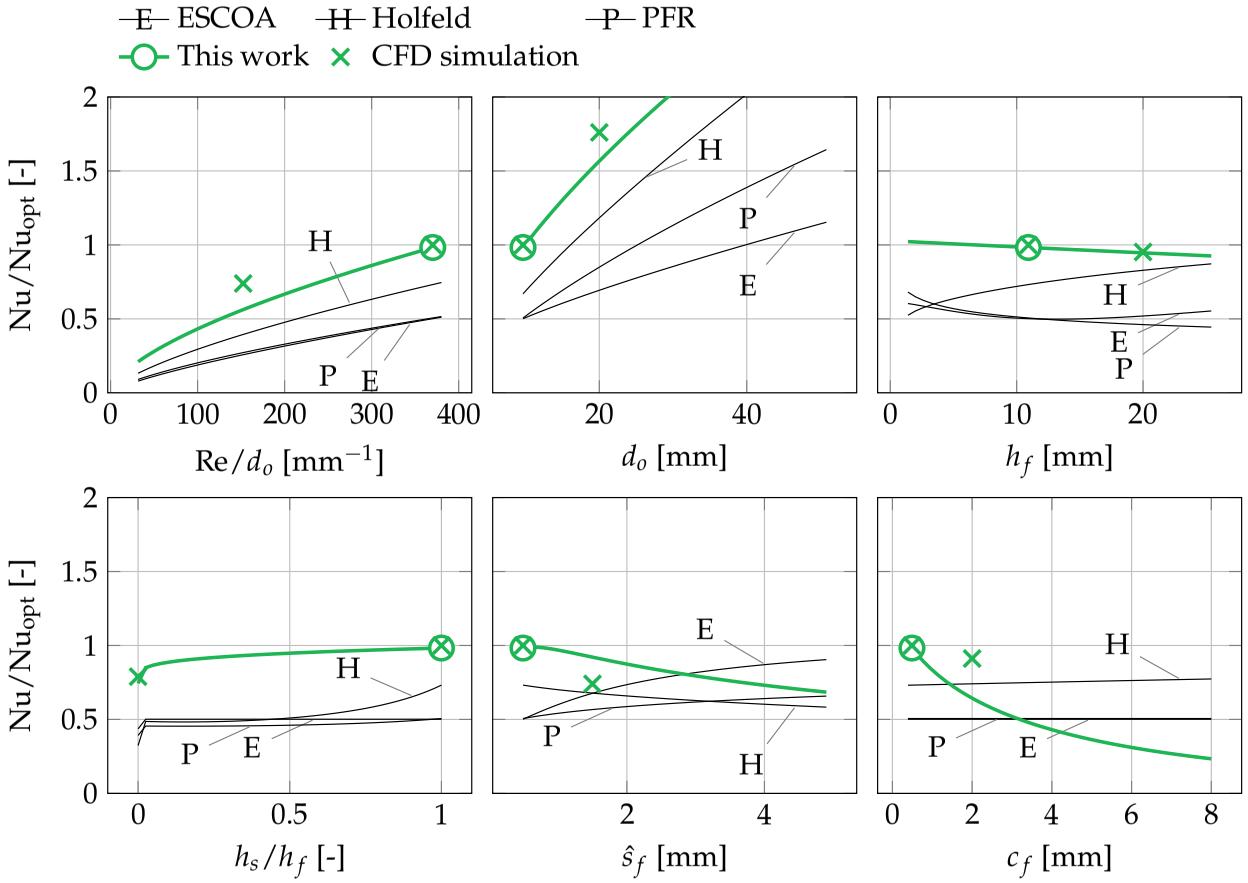

Figure 8. Trends in correlations around the case study optimum found using correlations developed in this work (marked by a circle). CFD simulations were independently sampled (not part of the dataset used for model development). Each parameter was varied independently, with remaining parameters held constant at the optimum.

Chapter 7

Paper 4 — Numerical modeling of vortex shedding in helically wound finned tube bundles in cross flow

Presented at the *16th International Heat Transfer Conference* in Beijing, China on 2018-08-11

This paper is not included due to copyright

Chapter 8

Conclusions and outlook

As stated in the introductory chapter, this thesis has developed, validated and used a CFD model to explore and expand the validity ranges of current thermal-hydraulic correlations for fin-tube bundles. Intermediate results include a solution method for a reduced domain model that utilizes the geometric periodicity of a tube bundle. The model has also been used to study transient flow, with application to vortex shedding prediction.

A quantitative approach has been taken; This work is the first in the fin-tube literature to show grid convergence and a quantitative comparison with experimental data simultaneously for the variables of engineering interest. Computational- and wall-time efficiency has also been a priority, both to enable the data-driven approach taken in the correlation development paper as well as to be able to compete with experimental work. The inaccuracies of existing correlations for small-diameter closely packed fin-tube geometries has been demonstrated, and new correlations with improved accuracy in this range have been developed.

Two weaknesses of the current approach are, firstly, that the sensitivity studies and subsequent (manual) data interpretations are relatively shallow. This has been motivated by the unknown relative influence among the parameters. By studying all parameters to some degree, it has been possible to rank the parameters in order of significance. This has been particularly important for the conclusions regarding the Nusselt number and fin efficiency: In Paper 2, results indicated that the standard fin efficiency calculation can be a large source of errors. In Paper 3 it was shown that the Nusselt number is almost exclusively a function of the Reynolds number and the tube diameter when an exact fin efficiency calculation is used. It is also the case that an automated study of the design space is much more time efficient than local sensitivity studies.

Secondly, it can be argued that the numerical model is relatively rudimentary and does not use advanced turbulence modeling concepts (e.g. large- or detached

eddy simulations). As discussed in chapter 3, the steady-state thermal-hydraulic predictions were relatively insensitive to the choice of eddy viscosity turbulence model and matched experimental data well. Hence, there was no need for excessive modeling detail. The vortex shedding predictions, on the other hand, deviated quite a bit from the values expected from literature correlations (see Paper 4). A sensitivity study with respect to the turbulence modeling strategy would indeed be very interesting, but it is probably more important to obtain good experimental data on vortex shedding in finned tubes to be used in validation.

In short, the conclusions from this work can be summed up as follows:

- CFD simulations can produce consistent data without uncertainties in fin efficiency and geometric details. Accuracy can be expected to be on par with experimental data, given that a good (converged) computational grid is used.
- Correlation building that uses adaptive sampling of CFD simulations in region of large uncertainty can achieve increased accuracy at a relatively moderate (computational- and labor-)cost.
- The improved correlations lead to a different thermal-hydraulic optimum with respect to heat exchanger weight when compared to the ESCOA correlation. This implies that correlation selection is important, and that the new correlations can influence future design choices if used.
- CFD simulations are able to predict certain phenomena more accurately than what is possible to include in correlations. One example is the influence of variable thermophysical properties. CFD therefore has a role in the heat exchanger development process, after thermal-hydraulic optimization but before experimental validation.
- Transient CFD simulations appear promising for prediction of phenomena related to flow induced vibration. Care should however be taken to properly validate models against experimental data and study the influence of turbulence model selection before exploring numerical studies further along these lines.

A few suggestions for further work can be made based on the findings in this work. First of all, the key findings should be validated experimentally. This includes, for example, the effect of thermophysical properties and the suggested compact design in Paper 3.

The data driven approach to correlation improvement seems to be a viable path considering that root-mean-square prediction errors for Euler and Nusselt numbers were decreased, in this work, by 46 % and 24 % respectively by increasing the dataset size by only 65 %. More data is one of three major components of increased model predictive accuracy in a broader machine learning context [1] (the other two being model capacity and computational power for model fitting). By

extrapolation, it is reasonable to assume that thermal-hydraulic correlations can be substantially improved by increasing the dataset size by an order of magnitude or so. Automated CFD simulations seems to be the only feasible path towards this goal.

The assumption of a uniform heat transfer coefficient should be reconsidered, for example by dividing the heat transfer area into active and non-active areas to account for the tube wake. A more specific model might improve the prediction accuracy of the heat transfer coefficient. An explicit model for bypassing flow should also be considered. The phenomenon is most certainly a nonlinear function of the tube bundle geometry, and will likely require a large amount of data unless a suitable theoretical simplification can be made. Models for uneven heat transfer coefficient and for bypassing flow would, however, enable a more accurate prediction of fin efficiency, compared to the theoretical model used today.

References

[1] Chen Sun et al. "Revisiting Unreasonable Effectiveness of Data in Deep Learning Era". In: *2017 IEEE Conference on Computer Vision (ICCV)*. 2017, pp. 843–852. arXiv: 1707.02968.

Appendices

Appendix A

Supplementary material to Paper 3

Table A.1: Data points from CFD simulations used for correlation development in Paper 3

Re [-]	d_o [mm]	h_f [mm]	h_s/h_f [-]	$\hat{s}_f$ [mm]	c_f [mm]	$\eta_{f,\mathrm{num}}$ [-]	Q_f [W]	Q_t [W]	$T_{b,\mathrm{in}}$ [K]	$T_{b,\mathrm{out}}$ [K]	Eu [-]	$\mathrm{NuPr}^{-1/3}$ [-]
5600	38.1	14.6	0.390	2.25	4.05	0.766	2.33	1.39e−1	315.9	306.5	1.79	64.1
6460	17.0	18.4	1.00	1.05	0.600	0.335	2.08	4.08e−2	317.6	311.5	2.32	83.6
2000	37.0	22.1	0.210	0.710	2.50	0.812	3.63e−1	2.58e−4	307.1	298.8	23.0	20.5
1420	28.1	9.34	0.	3.16	6.89	0.892	8.46e−1	8.42e−2	316.6	307.1	1.66	28.8
981	14.9	5.34	0.375	1.47	3.36	0.965	3.65e−1	1.61e−2	313.5	302.7	2.32	27.8
5010	13.5	10.0	0.	0.577	5.20	0.912	1.57	4.64e−3	312.7	302.0	2.70	61.7
8740	44.4	22.7	0.790	4.66	7.97	0.575	4.52	4.32e−1	320.2	315.9	0.984	68.9
1470	9.65	6.28	1.00	4.90	8.00	0.853	7.55e−1	1.73e−1	321.1	318.6	0.581	23.0
14 500	38.1	17.3	0.	2.42	5.53	0.649	4.59	3.38e−1	319.1	313.6	1.10	80.7
1740	34.7	8.17	0.610	0.490	0.500	0.962	2.28e−2	1.10e−5	300.3	298.0	31.5	35.1
1240	38.5	1.40	0.	0.490	8.00	1.00	3.05e−2	1.70e−4	320.1	313.5	0.955	5.05
1730	34.7	7.35	0.	0.490	4.06	1.00	1.21e−1	8.50e−5	315.9	306.6	6.25	5.40
524	11.7	4.83	0.188	1.48	4.04	0.959	2.41e−1	9.13e−3	313.2	302.3	2.55	20.4
1350	40.8	3.83	1.00	0.490	8.00	1.00	5.36e−2	8.80e−5	321.9	314.9	1.59	3.20
3640	9.65	6.28	1.00	4.90	8.00	0.787	1.20	2.98e−1	320.9	319.3	0.524	38.9
11 700	39.3	3.82	0.	0.753	0.400	0.961	3.86e−1	1.61e−2	307.9	298.6	3.26	139
6330	22.2	17.2	0.305	2.95	1.73	0.607	3.36	2.39e−1	319.2	314.1	1.11	55.1
841	12.8	5.34	0.	1.15	3.36	0.965	3.09e−1	6.29e−3	312.1	301.1	2.86	27.3
1420	28.1	12.5	0.	4.90	6.96	0.879	1.29	1.63e−1	317.9	310.2	1.25	26.0
3060	37.0	22.1	0.210	0.710	2.50	0.779	5.93e−1	4.46e−4	307.7	298.8	16.7	32.6
6540	23.8	16.7	0.100	1.37	2.75	0.599	2.71	9.83e−2	315.4	306.9	2.11	66.3
11 400	38.1	18.2	0.	2.25	4.05	0.641	4.13	2.67e−1	318.2	311.4	1.36	75.7
1360	15.1	9.00	0.	2.10	0.400	0.873	7.29e−1	3.52e−2	312.3	302.9	2.12	32.6
1730	34.7	7.35	0.102	0.491	0.390	0.954	2.00e−2	1.40e−5	300.3	298.0	34.2	34.0

4690	37.0	22.1	0.210	0.710	2.50	0.730	9.63e−1	8.19e−4	308.5	299.1	12.0	48.8
10 500	38.2	18.2	0.290	1.55	4.05	0.621	3.58	1.23e−1	315.8	306.9	2.03	90.1
9660	25.4	16.6	1.00	3.00	8.00	0.496	2.97	2.71e−1	320.8	317.9	0.949	74.3
5000	13.5	10.0	0.	1.15	5.20	0.903	2.09	7.98e−2	317.2	309.2	1.36	46.6
7410	27.0	15.9	0.153	1.37	1.85	0.535	2.44	9.82e−2	315.6	307.1	2.18	75.8
10 600	34.7	7.35	0.	0.490	4.06	0.946	8.50e−1	1.68e−3	315.5	304.7	3.62	45.2
5600	38.1	18.2	0.	2.25	4.05	0.689	2.74	1.51e−1	315.4	306.4	1.95	62.2
13 300	44.4	25.4	0.790	4.66	7.33	0.486	5.52	6.29e−1	320.2	317.0	0.866	86.7
3670	9.65	1.40	0.	4.45	8.00	0.981	2.74e−1	3.17e−1	321.3	319.9	0.504	35.1
1540	48.5	1.40	0.	4.90	8.00	0.987	1.30e−1	1.40e−1	318.9	312.1	0.722	21.2
6350	31.8	12.1	0.610	4.90	0.500	0.779	3.04	3.11e−1	318.5	312.5	0.902	69.8
1900	47.6	22.7	0.685	4.90	6.99	0.730	2.06	1.66e−1	315.9	306.7	1.89	38.3
4000	44.4	25.4	0.790	4.66	7.33	0.584	3.42	2.23e−1	318.7	312.4	1.36	51.7
1730	34.7	7.35	0.	4.90	0.400	0.983	6.98e−1	1.64e−1	314.1	304.1	1.63	38.4
2250	38.5	1.40	0.	0.490	8.00	1.00	4.76e−2	2.75e−4	322.3	316.6	0.830	6.87
3670	9.65	3.55	0.760	1.08	8.00	0.947	7.05e−1	6.00e−2	320.9	316.6	0.833	37.1
1510	29.8	12.5	0.	3.16	6.96	0.875	1.13	8.39e−2	315.3	305.5	1.87	31.2
16 700	48.5	1.40	0.	4.90	8.00	0.970	6.06e−1	6.10e−1	320.0	317.2	0.445	80.9
6060	24.3	18.0	0.	4.90	0.877	0.588	3.63	3.64e−1	319.9	316.0	0.847	50.2
1260	18.1	11.3	1.00	2.73	0.400	0.833	8.98e−1	3.46e−2	314.7	305.5	1.84	32.6
11 000	37.0	22.1	0.210	0.710	2.50	0.607	2.40	4.85e−3	310.7	300.7	6.12	93.2
4990	13.5	10.0	0.	4.62	5.20	0.913	2.56	3.53e−1	320.8	317.9	0.562	38.8
2930	33.1	10.9	0.	1.48	3.40	0.847	8.12e−1	2.10e−2	310.2	299.7	3.54	62.7
3670	9.65	13.9	1.00	1.03	0.400	0.409	1.41	2.76e−2	317.9	312.3	1.90	54.9
3670	9.65	8.34	1.00	0.490	0.390	0.637	7.34e−1	1.93e−3	311.3	301.6	3.66	70.7
7840	28.6	15.5	0.	0.848	2.87	0.706	1.95	1.25e−2	311.2	301.2	3.67	84.1
1810	18.1	9.76	1.00	2.73	1.83	0.847	1.03	8.79e−2	317.6	309.4	1.44	32.4
4900	16.1	11.3	1.00	4.00	0.500	0.648	1.92	3.15e−1	320.1	316.7	0.825	54.5
2650	30.1	10.9	0.	3.76	0.400	0.893	1.41	1.29e−1	315.5	306.5	1.53	42.1

7410	50.8	25.4	0.790	3.28	8.00	0.555	4.18	2.53e−1	318.4	311.7	1.51	71.4
11 000	32.4	8.29	1.00	0.490	7.13	0.702	1.11	3.95e−3	316.8	306.5	3.03	70.2
6730	17.7	10.0	1.00	3.39	8.00	0.761	2.38	2.85e−1	320.8	317.8	0.803	57.0
2000	25.0	13.8	0.790	3.56	6.20	0.843	1.67	1.19e−1	318.2	310.5	1.33	33.9
5000	13.5	10.0	0.	2.31	5.20	0.912	2.38	1.70e−1	319.8	314.9	0.817	40.4
2590	30.1	9.16	0.500	3.51	0.400	0.921	1.13	1.10e−1	315.5	306.0	1.48	42.6
1590	31.8	12.1	0.610	4.90	0.500	0.888	1.16	1.23e−1	315.7	306.5	1.55	33.3
7190	26.2	16.5	0.0763	2.16	2.75	0.553	2.82	2.18e−1	318.4	312.4	1.37	59.2
1810	18.1	9.76	1.00	2.73	0.600	0.794	1.00	5.10e−2	317.2	308.9	1.52	35.8
6770	23.8	15.7	0.	0.849	1.73	0.632	1.83	1.63e−2	311.1	301.5	3.70	78.5
7190	26.2	16.6	0.	1.37	2.75	0.513	2.53	1.03e−1	315.9	307.8	2.14	70.4
12 700	36.4	20.2	0.0500	0.490	4.75	0.492	1.76	4.72e−3	313.9	304.6	6.63	57.7
3320	9.70	3.70	0.	0.490	0.390	0.627	2.96e−1	9.98e−3	311.2	301.2	3.15	66.1
3740	9.65	7.88	0.316	0.490	0.400	0.301	5.71e−1	1.23e−2	315.0	306.8	3.74	62.2
3380	30.1	8.53	0.	1.48	0.490	0.832	6.23e−1	2.00e−2	308.8	299.4	3.18	74.5

Table A.3: Data points from CFD simulations used for correlation testing in Paper 3 (Latin Hypercube sample)

Re [-]	d_o [mm]	h_f [mm]	h_s/h_f [-]	$\hat{s}_f$ [mm]	c_f [mm]	$\eta_{f,\mathrm{num}}$ [-]	Q_f [W]	Q_t [W]	$T_{b,\mathrm{in}}$ [K]	$T_{b,\mathrm{out}}$ [K]	Eu [-]	$\mathrm{NuPr}^{-1/3}$ [-]
17 400	48.2	17.5	0.170	0.870	4.90	0.724	3.35	1.94e−2	312.7	302.2	3.30	121
2600	43.4	12.2	0.420	4.50	1.40	0.894	1.40	1.62e−1	315.5	305.8	1.60	42.6
2900	38.6	20.2	0.120	0.590	2.90	0.838	4.42e−1	2.54e−4	309.1	299.9	19.4	17.3
2370	47.4	19.8	0.590	4.84	3.10	0.761	2.03	1.89e−1	315.8	306.6	1.76	41.8
13 400	42.0	8.20	1.00	4.61	6.90	0.881	3.27	5.44e−1	320.6	316.0	0.731	90.9
4640	23.2	2.00	0.660	1.92	7.20	1.00	4.51e−1	1.05e−1	321.6	316.8	0.737	38.9
2980	13.0	14.4	0.160	4.21	2.30	0.729	2.55	2.58e−1	319.7	315.7	0.799	31.6
7150	37.0	22.1	0.210	0.710	2.50	0.676	1.54	1.78e−3	309.5	299.6	8.60	69.0
1320	26.3	4.90	0.	0.960	5.70	0.973	2.11e−1	1.05e−3	317.9	307.5	3.21	12.5
4360	25.0	13.8	0.790	3.56	6.20	0.791	2.58	1.95e−1	319.5	314.0	1.01	47.9
2360	44.8	12.9	0.610	1.70	6.60	0.894	8.12e−1	8.42e−3	311.3	300.1	4.21	46.6
4840	24.2	2.80	0.850	2.20	6.40	0.982	6.39e−1	1.35e−1	320.9	315.2	0.883	46.1
1600	10.0	6.20	0.310	2.90	1.50	0.912	9.02e−1	1.15e−1	318.4	311.8	1.04	28.8
1310	28.8	20.9	0.0700	4.11	4.60	0.713	1.69	1.20e−1	315.2	306.3	1.94	28.4
1490	40.2	4.30	0.680	2.06	1.90	0.985	1.80e−1	1.58e−2	309.2	299.1	3.58	40.3
9260	37.7	18.9	0.460	1.46	4.20	0.609	3.31	8.27e−2	315.0	305.8	2.30	90.9
3930	11.5	9.20	0.700	2.42	7.70	0.790	1.70	1.53e−1	320.3	316.9	0.773	39.1
1280	32.0	3.10	0.290	4.45	1.20	1.00	2.30e−1	9.74e−2	313.6	303.0	1.58	31.4
620	18.9	11.4	0.950	3.95	2.90	0.880	6.55e−1	5.66e−2	315.7	306.6	1.76	20.7
3890	30.6	23.6	0.750	1.63	3.70	0.544	2.35	3.11e−2	313.8	304.3	3.00	66.6
8760	29.5	24.6	0.390	2.65	4.40	0.466	4.36	2.85e−1	319.1	314.5	1.23	65.5
6550	17.7	9.70	0.900	3.66	3.50	0.779	2.37	3.51e−1	320.1	316.4	0.800	62.0
2120	19.6	7.40	0.	3.78	5.60	0.932	1.04	1.78e−1	319.6	313.6	0.951	29.6
2870	46.5	24.0	0.530	2.34	7.40	0.769	2.03	2.77e−2	311.5	301.0	3.36	57.7

793	15.4	15.1	0.470	3.30	7.80	0.791	1.14	6.99e−2	317.0	309.2	1.49	19.8
4170	15.0	16.4	0.810	2.79	5.90	0.579	2.40	1.64e−1	320.0	316.4	0.946	43.5
3040	33.8	16.9	0.260	3.21	5.30	0.754	2.15	1.66e−1	316.7	308.1	1.63	43.4
2940	50.6	6.10	0.540	1.23	5.00	0.955	3.60e−1	3.80e−3	313.7	302.8	3.54	27.4
850	21.3	10.7	0.360	3.09	3.90	0.895	6.97e−1	5.33e−2	313.9	303.9	2.08	25.3
1540	35.5	22.2	0.910	1.21	2.00	0.808	4.77e−1	6.21e−4	306.3	298.2	10.8	51.4